JEM Journal of Experimental Medicine

ARTICLE

Neuronal Epac1 mediates retinal neurodegeneration in mouse models of ocular hypertension

Wei Liu[1,2], Yonju Ha[1], Fan Xia[1], Shuang Zhu[1], Yi Li[1], Shuizhen Shi[1], Fang C. Mei[3], Kevin Merkley[1], Gianmarco Vizzeri[1], Massoud Motamedi[1], Xiaodong Cheng[3], Hua Liu[1], and Wenbo Zhang[1,4]

Progressive loss of retinal ganglion cells (RGCs) leads to irreversible visual deficits in glaucoma. Here, we found that the level of cyclic AMP and the activity and expression of its mediator Epac1 were increased in retinas of two mouse models of ocular hypertension. Genetic depletion of Epac1 significantly attenuated ocular hypertension–induced detrimental effects in the retina, including vascular inflammation, neuronal apoptosis and necroptosis, thinning of ganglion cell complex layer, RGC loss, and retinal neuronal dysfunction. With bone marrow transplantation and various *Epac1* conditional knockout mice, we further demonstrated that Epac1 in retinal neuronal cells (especially RGCs) was responsible for their death. Consistently, pharmacologic inhibition of Epac activity prevented RGC loss. Moreover, in vitro study on primary RGCs showed that Epac1 activation was sufficient to induce RGC death, which was mechanistically mediated by CaMKII activation. Taken together, these findings indicate that neuronal Epac1 plays a critical role in retinal neurodegeneration and suggest that Epac1 could be considered a target for neuroprotection in glaucoma.

Introduction

Glaucoma, a neurodegenerative disease of the eye, is a leading cause of irreversible blindness, affecting >70 million people worldwide (Chen et al., 2018). It is a group of heterogeneous disorders characterized by the progressive loss of retinal ganglion cells (RGCs) and damage of their axons. Since RGCs cannot regenerate, their death results in irreversible visual loss. High intraocular pressure (IOP) is considered the most important risk factor for this disease and is the only treatable target for management of glaucoma. However, lowering IOP is not always effective to prevent visual loss in all glaucoma patients (Chen et al., 2018; Varma et al., 2008). Thus, there is an unmet need to identify the underlying mechanisms of neurodegeneration and develop neuroprotective strategies to prevent RGC loss and disease progression in glaucoma.

cAMP is one of the most common and universal second messengers and has been previously associated with protein kinase A to regulate many pathophysiological processes (Cheng et al., 2008; Taylor et al., 2013). Exchange protein activated by cAMP (Epac) is a newly identified mediator of cAMP. Upon cAMP binding, Epac is activated and induces the activation of Ras-like GTPase family members Rap1 and Rap2 (de Rooij et al., 1998; Kawasaki et al., 1998). Acting through small GTPases, Rap1 and Rap2, Epac links cAMP signaling to calcium mobilization, kinases activation, gene transcription, and cytoskeleton dynamics to regulate cellular functions such as cell proliferation, death, and hypertrophy (Robichaux and Cheng, 2018; Schmidt et al., 2013). Two isoforms of Epac have been identified, namely Epac1 and Epac2 (Chen et al., 2014). Epac1 is ubiquitously expressed in tissues and often involved in pathologic conditions such as cardiac hypertrophy, heart failure, pain perception, and obesity, while Epac2 regulates physiological processes including insulin secretion, learning, and memory (Breckler et al., 2011; Okumura et al., 2014; Srivastava et al., 2012; Wang et al., 2013; Yan et al., 2013; Zhang et al., 2009). In the retina, Epac1 is expressed in retinal layers containing neurons (Whitaker and Cooper, 2010), but its pathophysiological role is largely unknown.

In this study, we found that the level of cAMP and the activity and expression of Epac1 were increased in two glaucoma-relevant mouse models induced by ocular hypertension; therefore, we examined if targeting the cAMP-Epac1 signaling pathway would affect degenerative retinopathy in these models. Our study demonstrated that genetic deletion of *Epac1* globally or specifically in retinal neurons, particularly in RGCs, decreased

[1]Department of Ophthalmology & Visual Sciences, University of Texas Medical Branch, Galveston, TX; [2]Department of Ophthalmology, Union Hospital, Tongji Medical College, Huazhong University of Science and Technology, Wuhan, China; [3]Department of Integrative Biology and Pharmacology, Texas Therapeutics Institute, University of Texas Health Science Center at Houston, Houston, TX; [4]Departments of Neuroscience, Cell Biology & Anatomy, University of Texas Medical Branch, Galveston, TX.

Correspondence to Wenbo Zhang: we2zhang@utmb.edu; Hua Liu: hualiu@utmb.edu.

vascular inflammation, reduced neuronal apoptosis and necroptosis, and finally protected against RGC loss and dysfunction induced by elevated IOP. Furthermore, pharmacologic inhibition of Epac was neuroprotective, and Epac1 activation exerted neurotoxic effects through Ca^{2+}/calmodulin-dependent protein kinase II (CaMKII). These results suggest that neuronal Epac1 is a potential target for novel neuroprotective therapies in glaucoma pathogenesis.

Results

cAMP/Epac pathway is activated and induces neurodegeneration in retinal ischemia-reperfusion (IR) injury

To address the pathological role of Epac1 in glaucoma, we used a mouse IR model in which retinal ischemia is induced by a transient increase of IOP and neuronal cell death occurs within a few hours to 1 wk (Chi et al., 2014; Ha et al., 2015; Skowronska-Krawczyk et al., 2015). This model has been widely used to study mechanisms of RGC death and neuroprotection in retinopathies including acute glaucoma (Chi et al., 2014; Ha et al., 2015; Hartsock et al., 2016; Li et al., 2018; Skowronska-Krawczyk et al., 2015; Sun et al., 2010; Wan et al., 2017). We first examined the activation and expression of Epac1 in retinas of WT mice after retinal ischemia. Our results showed that cAMP, the upstream activator of Epac1, was up-regulated especially in the cells of the ganglion cell layer (GCL) 3 h after ischemia compared with sham control (Fig. 1 A). The activity level of Epac direct downstream effector, Rap1-GTP, was markedly increased 3 h after ischemia (Fig. 1 B), suggesting that Epac signaling is activated at this time point. Other indirect downstream targets of Epac signaling including AKT (protein kinase B) and ERK were also activated after ischemia (Fig. S1 A). Additionally, the levels of Epac1 mRNA and protein were increased 12–24 h after ischemic injury, and Epac1 was mainly localized in the GCL (Fig. 1, C–E). In contrast, Epac2 expression was decreased (Fig. 1 D). These observations signify that the cAMP/Epac1 pathway may be implicated in IR.

To test this possibility, we used *Epac1*$^{-/-}$ mice that are fertile and show no obvious morphological abnormalities. Their eyes exhibit normal retinal structure upon histological examination (Fig. S1 B) and normal retinal neuronal function as determined by electroretinography (ERG; Fig. S1 C). Epac1 protein ablation in the retina of *Epac1*$^{-/-}$ mice was validated by Western blot, and its deficiency did not cause a compensatory change in Epac2 (Fig. S1, D and E). We next subjected *Epac1*$^{-/-}$ mice and age-matched WT mice to IR and examined retinal cell death shortly after retinal ischemia by TUNEL (terminal deoxynucleotidyl transferase dUTP nick end labeling) assay. Compared with WT sham control, TUNEL staining was largely increased in neurons in the GCL and inner nuclear layer (INL) of WT retinas 12 h (Fig. 2 A) and 24 h after ischemia (Fig. S1 F), which is consistent with previous studies (Ha et al., 2015; Nishijima et al., 2007). In contrast, the number of TUNEL-positive cells was significantly reduced in *Epac1*$^{-/-}$ retinas after ischemic injury, whereas it was similar in both genotypes at baseline (Fig. 2 A and Fig. S1 F).

Increasing evidence has demonstrated the importance of necroptosis in retinal cell death (Cai et al., 2015; Do et al., 2017; Dvoriantchikova et al., 2014; Shosha et al., 2016); therefore, we examined the effect of *Epac1* deletion on necroptosis. At the molecular level, necroptosis is reported to be regulated by receptor-interacting protein 3 (RIP3), whose activation is tightly regulated by phosphorylation. We examined the phosphorylation level of RIP3 before and after ischemic injury in both WT and *Epac1*$^{-/-}$ mice and observed that phosphorylated RIP3 (pRIP3) was markedly increased in WT ischemic retinas, which was blunted by Epac1 deficiency after injury (Fig. 2 B). Since plasma membrane permeability is an early hallmark of necroptotic cell death, we further used propidium iodide (PI), which cannot cross the intact membrane of live cells but can cross disrupted cell membrane, to detect necroptotic cells (Liu et al., 2019; Shosha et al., 2016; Unal Cevik and Dalkara, 2003). We found that PI-positive cells were dramatically increased in the GCL and INL of WT retinas within 12 h following ischemic injury in comparison to WT sham control, whereas *Epac1* deletion reduced the number of necroptotic cells after retinal ischemia (Fig. 2 C). Combined, these observations imply that Epac1 up-regulation mediates retinal neuronal death after ischemic injury through apoptosis and necroptosis.

Epac1 deletion results in reduced retinal vascular inflammation and permeability following retinal ischemia

Following ischemic injury, vascular inflammation and leakage occur within 24 h and play critical roles in further neuronal injury (Ha et al., 2015; Zhang et al., 2017). To assess the effects of Epac1 genetic ablation in these processes, we perfusion-labeled vessels and leukocytes attached to vessels with concanavalin A (Con A; leukostasis assay) together with CD45 staining to identify all leukocytes in the retinas of WT and Epac1-deficient mice (Liu et al., 2019; Rojas et al., 2010). As demonstrated in Fig. 3, A–C (for central retina) and Fig. S2 (for peripheral retina), leukocyte attachment to retinal vessels (Con A^+, $CD45^+$ cells) and infiltration into the retina (Con A^-, $CD45^+$ cells), which are hallmarks of vascular inflammation, were significantly increased in WT mice 24 h after retinal ischemia. Such increases were substantially abrogated by *Epac1* deletion. Moreover, to test the effect of Epac1 genetic ablation on vascular leakage, we injected FITC-BSA and measured albumin leakage from vessels to neuronal retina after ischemic injury. We found that Epac1 deficiency significantly inhibited ischemia-induced vascular leakage in the retina (Fig. 3 D), although it slightly increased the baseline of vascular permeability in sham eyes, which is consistent with previous reports (Curry et al., 2019; Kopperud et al., 2017).

Blockade of Epac1 prevents high IOP-induced retinal neurodegeneration

7 d after retinal ischemia, high-resolution spectral-domain optical coherence tomography (OCT) analysis revealed that the thickness of ganglion cell complex (GCC, including nerve fiber layer; GCL, and inner plexiform layer; Yang et al., 2012a) was dramatically reduced in ischemia-injured WT mice compared with WT sham controls, indicating degeneration of RGCs and their axons. However, GCC thickness was significantly preserved in ischemia-injured *Epac1*$^{-/-}$ mice (Fig. 4 A). To further assess the impact of *Epac1* deletion on ischemic injury–induced

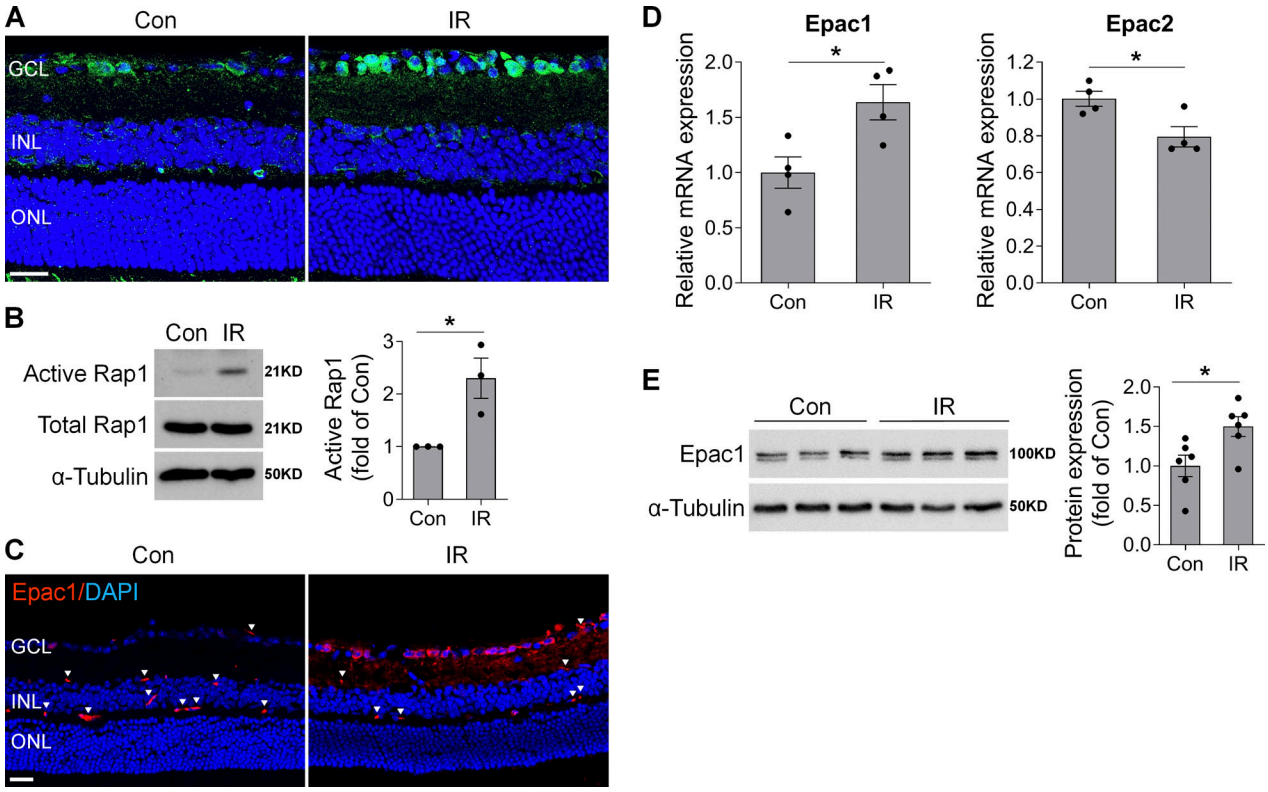

Figure 1. **cAMP/Epac1 signaling is increased in mouse model of IR injury.** WT mice were subjected to IR injury, and retinas or eyeballs were collected at various times after IR. **(A)** Representative images of cAMP immunostaining (green) in retinal frozen sections from control (Con) and injured eyes 3 h after IR. Blue, DAPI staining. *n* = 4 mice. **(B)** Active Rap1 was assessed by pull-down assay in control and injured retinas 3 h after IR, followed by Western blotting with anti-Rap1 antibody. One representative blot from three independent experiments was shown. Graph represents relative amount of active Rap1. *n* = 3 mice. **(C)** Epac1 immunostaining (red) in retinal sections from control and injured eyes 12 h after IR. Blue, DAPI staining. Arrowheads indicate nonspecific staining on vessels. *n* = 3–4 mice. **(D and E)** Epac1 and Epac2 mRNA expression by quantitative PCR (*n* = 4 mice; D) and Epac1 protein expression by Western blotting (*n* = 6 mice; E) in noninjured control retinas or injured retinas 24 h after IR. *, P < 0.05; Student's *t* test. Scale bar: 20 µm. ONL, outer nuclear layer. Error bars represent SEM.

loss of RGCs, we stained retinal flatmounts with antibody against Tuj1, which is a marker of RGCs. Consistently, there was a marked decrease in the number of Tuj1-positive cells in WT retina 7 d (Fig. 4 B), as well as at a longer time point (14 d; Fig. S3) after retinal ischemia compared with WT sham control, and *Epac1* deletion significantly blunted this effect at both time points, suggesting that *Epac1* deletion indeed protects RGCs from cell death rather than just delaying cell apoptosis. To assess the effect of *Epac1* deletion on the function of the inner retina, we used dark-adapted (scotopic) ERG to record the a-wave, b-wave, and positive scotopic threshold response (pSTR), which reflect the functions of photoreceptor, bipolar cells, and RGCs, respectively (Ha et al., 2017, 2018; Liu et al., 2019; Saszik et al., 2002). These analyses showed that the amplitudes of a-wave, b-wave, and pSTR were all significantly reduced in WT mice 14 d after retinal ischemia compared with WT sham mice (Fig. 4 C). However, in mice with *Epac1* deletion, b-wave and pSTR amplitudes after IR were statistically different from those of WT after IR, indicating a degenerative effect of Epac1 on bipolar cells and RGCs.

Encouraged by the neuroprotective effect of *Epac1* deletion, we further tested whether pharmacologic blockade of Epac can be used to alleviate RGC injury after retinal ischemia. WT mice were treated with ESI-09, a potent inhibitor of Epac signaling (20 mg/kg, i.p.; Ye et al., 2015; Zhu et al., 2015) or vehicle solution (PBS containing 10% Tween-80 and 20% ethanol, i.p.) 6 h before inducing high IOP and continuously injected once a day for 7 d. ESI-09 partially reduced Epac activity after ischemic injury (Fig. 5 A) and, remarkably, prevented RGC loss 7 d after retinal ischemia (Fig. 5 B). Altogether, these results suggest that Epac1 is a transducer of retinal neuronal death and that blocking Epac1 is a promising approach for neuroprotection.

Epac1 in resident retinal cells mediates neurodegeneration after retinal ischemia

After retinal ischemia, infiltration of bone marrow (BM)–derived leukocytes to the injured eye occurs and contributes to neuronal damage in the retina (Ha et al., 2015, 2017). Since Epac1 is also expressed in leukocytes (Lorenowicz et al., 2006; Scott et al., 2016), we aimed to determine whether Epac1 expressed in BM-derived cells or Epac1 expressed in retinal cells contribute to ischemic injury–induced retinal neuronal damage. We made BM chimeras in which WT mice were lethally irradiated, with a lead shield used to protect the head and eyes, and BM was reconstituted with *Epac1*$^{-/-}$ (*Epac1*$^{-/-}$→WT) or WT (WT→WT) BM

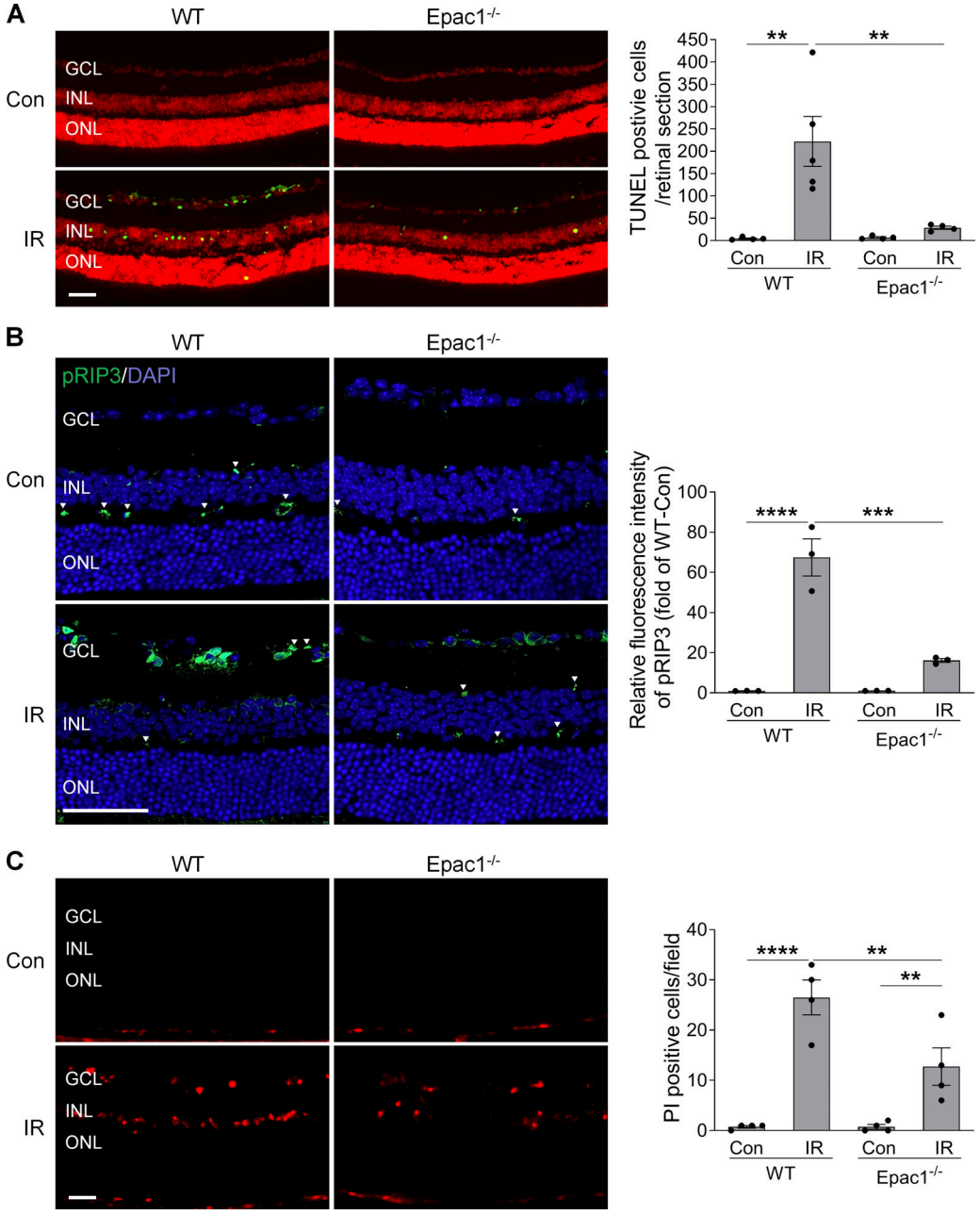

Figure 2. ***Epac1* deletion reduces both apoptotic and necroptotic cell death after IR injury. (A)** TUNEL assay was conducted on retinal frozen sections 12 h after IR in WT and *Epac1*$^{-/-}$ mice. Green, TUNEL-positive cells; red, PI staining of nuclei. *n* = 4–5 mice; TUNEL-positive cells in three retinal sections for each sample were counted under microscope and calculated as average value. **(B)** RIP3 phosphorylation (green) in retinal sections from WT and *Epac1*$^{-/-}$ mice 12 h after IR. Blue, DAPI staining. Arrowheads indicate nonspecific staining on vessels. Bar graph represents the intensity of pRIP3. *n* = 3 mice; immunostaining intensity was quantified from three independent observed areas of each retinal section and averaged. **(C)** Representative images of PI-labeled necroptotic cells (red) in retinal frozen section. PI was injected i.p. 9 h after IR, and eyeballs were collected 3 h after PI injection for retinal section. Bar graph represents the number of PI-positive cells per field. *n* = 4–5 mice; PI-positive cells from three independent observed areas of each retinal section were counted. For each eye, data from three sections were averaged, and the mean of four to five eyes was used as the representative value for each group. **, P < 0.01; ***, P < 0.001; ****, P < 0.0001; one-way ANOVA. Scale bar: 50 µm. ONL, outer nuclear layer. Error bars represent SEM.

cells. In a similar manner, we created WT→*Epac1*$^{-/-}$ or *Epac1*$^{-/-}$→*Epac1*$^{-/-}$ chimeras (Fig. 6 A). These chimeric mice were subjected to retinal ischemic injury 6 wk after BM transplantation. 7 d after retinal ischemia, compared with WT→WT (control) mice, the loss of GCC thickness and RGC number was decreased in WT→*Epac1*$^{-/-}$ (Epac1 was intact in leukocytes and deleted in retinal cells) and *Epac1*$^{-/-}$→*Epac1*$^{-/-}$ (Epac1 was deleted in both leukocytes and retinal cells) but not in *Epac1*$^{-/-}$→WT (Epac1 was deleted in leukocytes and intact in retinal cells; Fig. 6, B and C). These results indicate that Epac1 expressed in resident retinal cells but not in BM-derived cells is the major effector that promotes RGC injury after retinal ischemia.

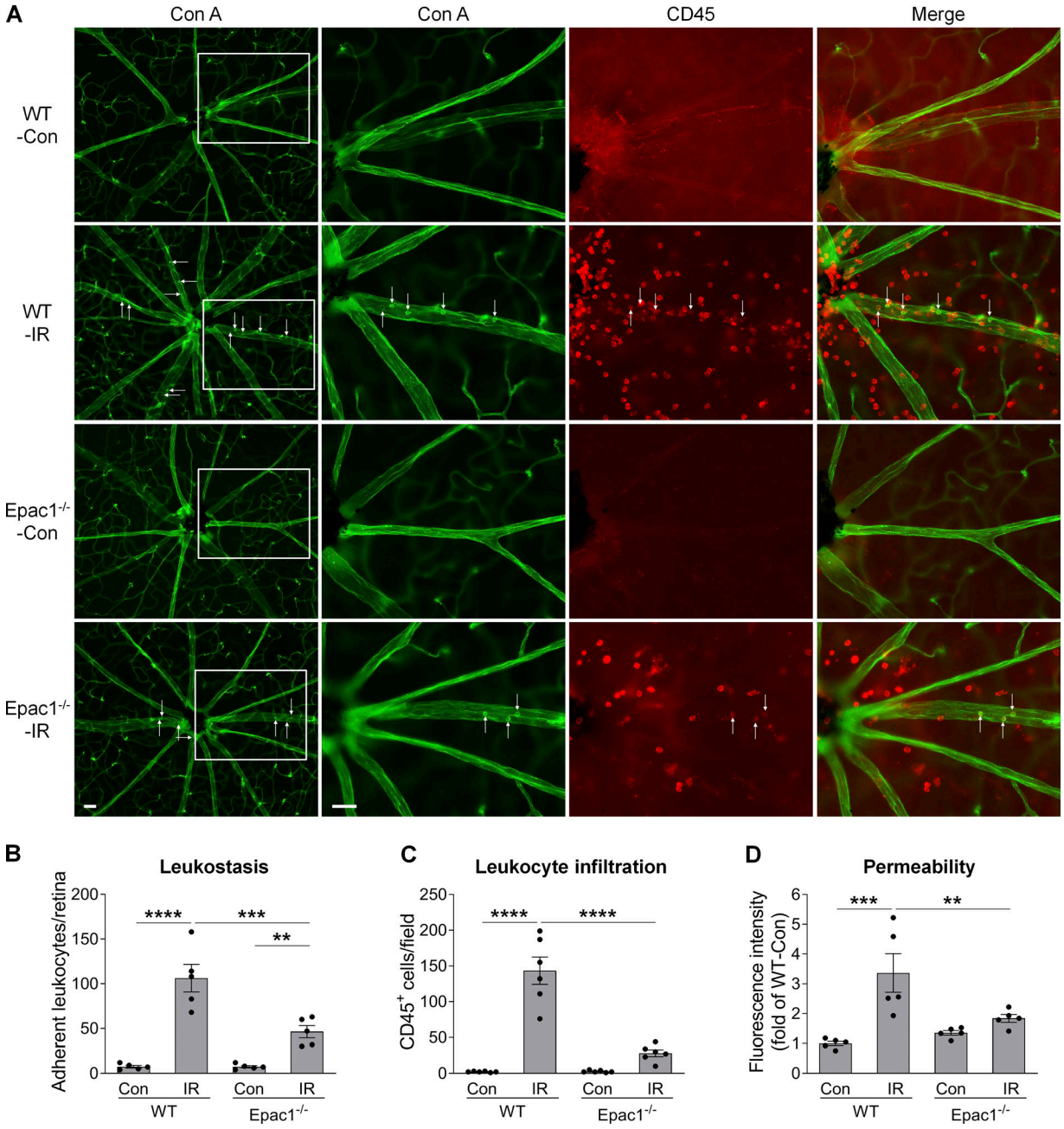

Figure 3. ***Epac1* deletion decreases leukostasis and permeability in the retina after IR injury.** WT and *Epac1*$^{-/-}$ mice were subjected to IR, and leukostasis assay or permeability assay was performed 24 h after IR. **(A)** Representative images of leukostasis in the central retinas. Green, Con A–labeled retinal vasculature and adherent leukocytes; red, CD45 immunostaining for leukocytes. Rectangles in the left rows of images are zoomed in, and arrows indicate stationary leukocytes adherent to the vascular endothelium. Scale bar: 50 µm. **(B and C)** Bar graphs represent the number of leukocytes adherent to the retinal vasculature (Con A$^+$, CD45$^+$) per retina and infiltrated leukocytes (Con A$^-$, CD45$^+$) per field (four images were taken randomly for each eye and calculated as average value). *n* = 5–6 mice. **(D)** Quantification of permeability 24 h after IR. *n* = 5 mice. **, P < 0.01; ***, P < 0.001; ****, P < 0.0001; one-way ANOVA. Error bars represent SEM.

Epac1 in microglia/myeloid cells and astrocytes is dispensable for RGC injury after retinal ischemia

Epac1 is expressed in many retinal cell types (Whitaker and Cooper, 2010). To delineate in which cell type Epac1 expression is responsible for ischemic injury–induced retinal neuron death, we conditionally deleted *Epac1* in myeloid/microglia and astrocytes using the Cre-loxP system. The "floxed" allele has loxP sites flanking the third to sixth exons of the *Epac1* gene (Yang et al., 2012b). To monitor Cre recombinase activity, Cre mice were bred with the Rosa26YFP reporter strain (Srinivas et al., 2001), in which YFP expression will occur upon removal of a floxed intervening segment by Cre recombinase. We first intercrossed *Epac1*$^{flox/flox}$ mice with LysM-Cre mice to generate a myeloid-specific knockout of *Epac1* (LysM-Cre; *Epac1*$^{fl/fl}$; Clausen et al., 1999). In the retina, the YFP expression pattern showed that Cre activity was confined to Iba1-positive cells (microglia;

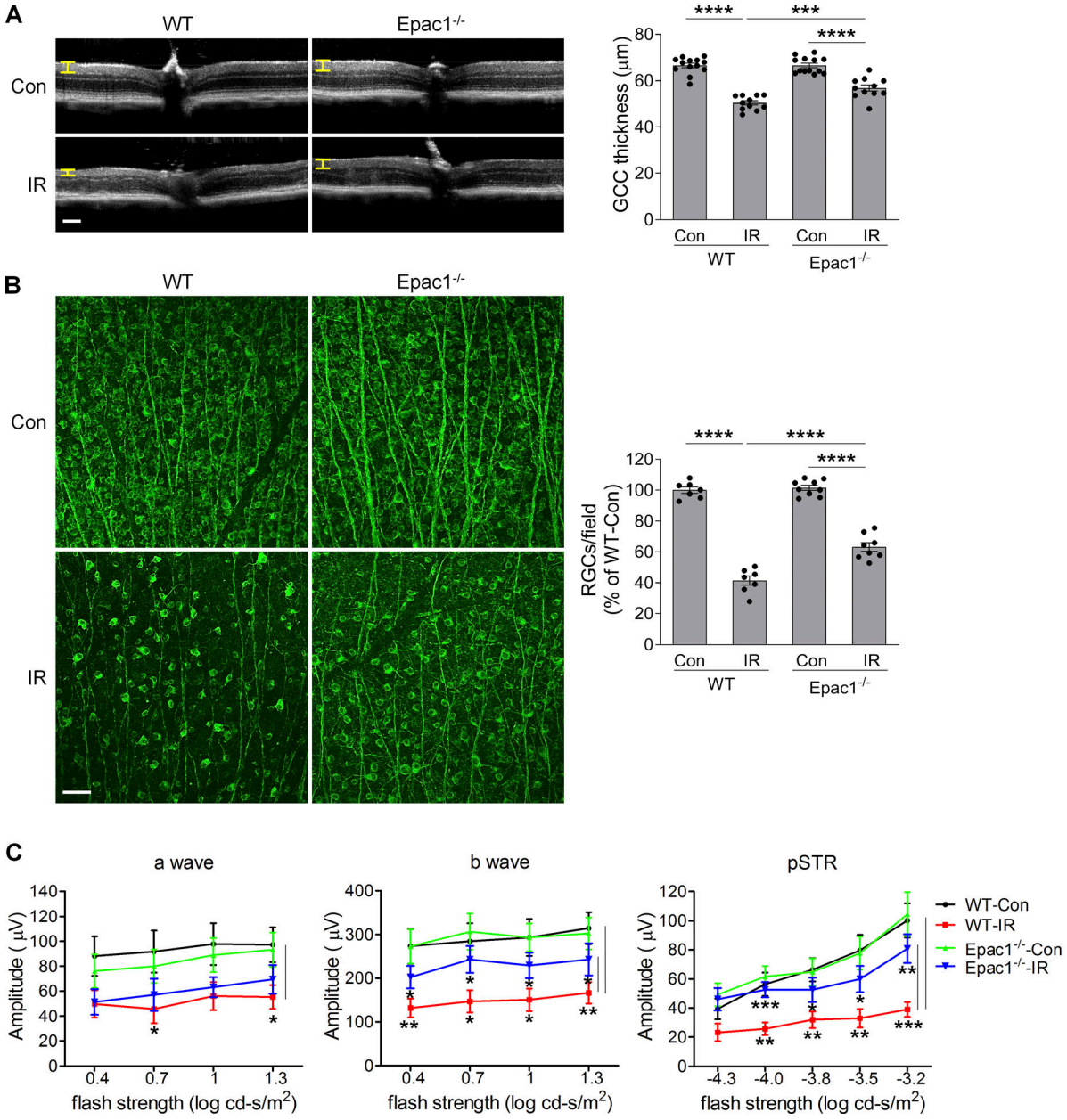

Figure 4. ***Epac1* deletion prevents cellular/functional loss of RGCs after IR injury. (A)** OCT analysis was performed in live WT and *Epac1*$^{-/-}$ mice for retinal thickness 7 d after IR. Yellow H lines indicate the thickness of GCC (composed of the retinal nerve fiber layer, GCL, and inner plexiform layer). Bar graph represents the thickness of GCC. *n* = 11–13 mice. Scale bar: 100 µm. **(B)** Representative images of retinal flatmounts labeled with Tuj1 antibody (green) 7 d after IR in WT and *Epac1*$^{-/-}$ mice. Bar graph represents the percentage of Tuj1-positive cells per field relative to WT control retinas (WT-Con). Scale bar: 50 µm. *n* = 7–9 mice; eight images were taken at the peripheral retina for each sample and calculated as average value. ***, P < 0.001; ****, P < 0.0001; one-way ANOVA. **(C)** ERG analysis 14 d after IR. Graphs represent average amplitudes of a-wave, b-wave, and pSTR over a range of stimulus strengths. *n* = 11–15 mice. *, P < 0.05; **, P < 0.01; ***, P < 0.001; Student's *t* test for each time point. Error bars represent SEM.

Fig. S4 A). However, deletion of *Epac1* on myeloid cells did not abrogate GCC thinning and RGC loss 7 d after retinal ischemia (Fig. S4, B and C). We further conditionally deleted *Epac1* in astrocytes with GFAP-Cre. The YFP expression pattern showed that Cre activity was confined to the astrocytes in uninjured retina (Fig. S5 A). Nevertheless, deletion of *Epac1* in astrocytes also did not abrogate GCC thinning and RGC loss at 7 d after retinal ischemia (Fig. S5, B and C). Taken together, these results indicate that Epac1 in microglia/myeloid cells and astrocytes is dispensable for ischemic injury–induced retinal neurodegeneration and is not a major mediator of RGC death.

Epac1 in RGCs mediates high IOP–induced retinal neurodegeneration

Synapsin 1 (Syn1) is a neuron-specific synaptic vesicle protein expressed in neurons of retinal GCL and developing INL (Haas et al., 1990). By crossing Syn1 promoter–driven Cre mice (Syn1-Cre) with Rosa26YFP reporter mice, we found that YFP was

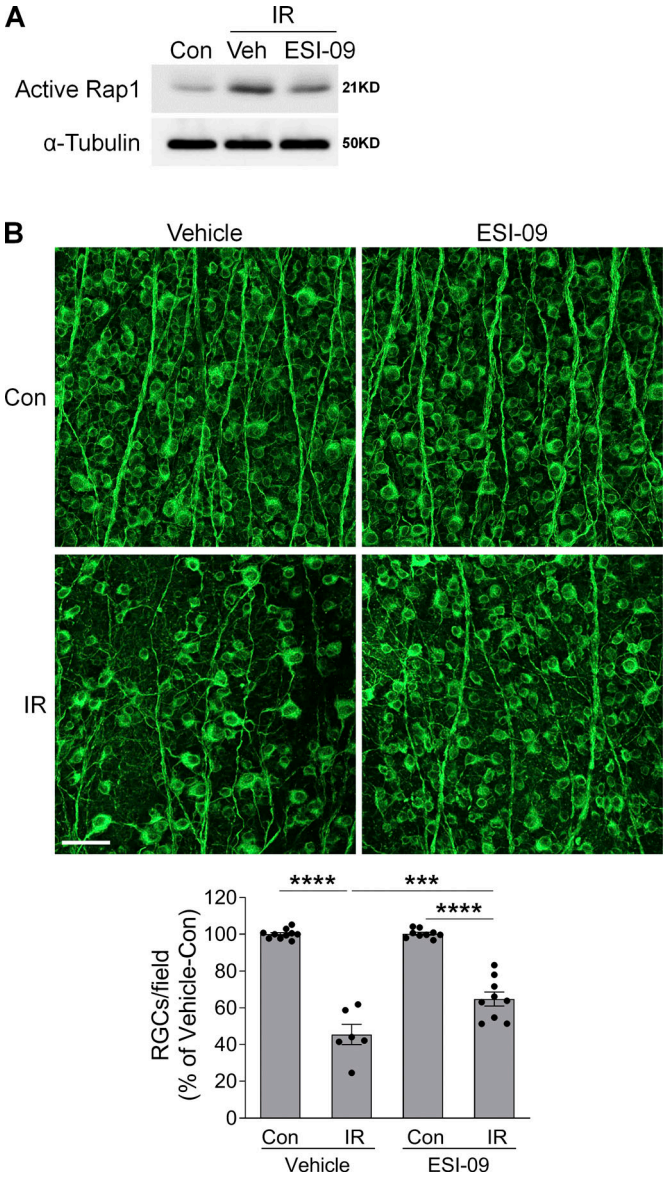

Figure 5. **Epac inhibitor prevents RGC loss after IR injury. (A)** Active Rap1 in control and injured-retinas from vehicle (Veh) or ESI-09–treated WT mice 3 h after IR. *n* = 3. **(B)** Representative images of retinal flatmounts labeled with Tuj1 antibody (green) 7 d after IR in vehicle- or ESI-09-treated WT mice. Bar graph represents the percentage of Tuj1-positive cells per field relative to vehicle-treated control retinas. Scale bar: 50 µm. *n* = 6–10 mice; eight images were taken at the peripheral retina for each sample and calculated as average value. ***, P < 0.001; ****, P < 0.0001; one-way ANOVA. Error bars represent SEM.

predominantly localized in RGCs and some inner neurons in the INL but not in astrocytes, vascular cells, or Müller cells (Fig. 7, A and B), indicating that Syn1-Cre can be used to specifically delete loxP-flanked genes in RGCs and some inner neurons. Therefore, in order to investigate the role of Epac1 expressed in RGCs in retinal neuronal injury, we crossed *Epac1*$^{flox/flox}$ mice with Syn1-Cre mice to specifically delete Epac1 in RGCs (*Epac1*$^{RGC\text{-}KO}$: Syn1-Cre; *Epac1*$^{fl/fl}$). We then subjected *Epac1*$^{flox/flox}$ and *Epac1*$^{RGC\text{-}KO}$ mice to retinal ischemic injury and observed that deletion of *Epac1* in RGCs significantly abrogated GCC thinning and RGC loss 7 d after retinal ischemia (Fig. 7, C and D), which is similar to the aforementioned results from global *Epac1* KO mice (Fig. 4, A and B). Collectively, our data indicate that Epac1 deficiency in RGCs is indeed responsible for their increased survival in the IR model. Interestingly, vascular inflammation in *Epac1*$^{RGC\text{-}KO}$ mice was also significantly reduced (Fig. 8), suggesting that Epac1 expression in RGCs not only drives RGC death but also affects retinal inflammation, likely through the cross-talk between RGCs and their interacting vascular beds.

Epac1 induces RGC death through CaMKII

To determine potential mechanisms by which Epac1 induces RGC death, we performed in vitro experiments with primary RGC cultures using the two-step immunopanning technique (Ha et al., 2015, 2017, 2018). When primary RGCs were challenged with 8-pCPT-2-O-Me-cAMP-AM (007-AM), a selective Epac agonist prodrug with enhanced cell-permeable potency to induce Epac activation (Vliem et al., 2008), it dramatically induced the death of RGCs isolated from WT mice but not those from *Epac1*$^{-/-}$ mice (Fig. 9 A), suggesting that Epac activation is sufficient to induce RGC death and that the effect of 007-AM is mainly mediated by Epac1. CaMKII, a serine-threonine kinase, is one of the major downstream targets that mediate the biological effects of Epac (Liu and Schneider, 2013; Métrich et al., 2008; Ohnuki et al., 2014; Pereira et al., 2007, 2015). Upon 007-AM treatment, CaMKII activity was increased in RGCs (Fig. 9 B). As a means to define the downstream molecule that was responsible for Epac1 activation–induced RGC death, we treated RGCs with 007-AM in the presence of CaMKII inhibitor (KN93, 1 µM) together with inhibitors that block other potential downstream targets of Epac, including p38MAPK (SB202190, 10 µM), JNK (JNK inhibitor, 10 µM), protein kinase C (GF109203X, 100 nM), and PI3K/AKT (LY294002, 10 µM). After examining cell death by TUNEL assay, we observed that CaMKII inhibitor KN93 robustly abrogated the ability of 007-AM–induced RGC death (Fig. 9 C).

To determine the potential involvement of CaMKII in Epac1-mediated RGC injury in vivo, we examined the phosphorylation levels of CaMKII in the retinas of WT and *Epac1*$^{-/-}$ mice 3–24 h after retinal ischemia. We found that phosphorylation of CaMKII was increased in WT retinas after ischemic injury (Fig. 9, D and E), while its activation was suppressed by *Epac1* deletion (Fig. 9 E). Furthermore, the administration of CaMKII inhibitor KN93 to WT mice significantly attenuated IR-induced RGC loss, which recapitulates the phenotype found in *Epac1*$^{-/-}$ mice (Fig. 9 F). These data suggest that CaMKII is a key mediator of Epac1-mediated RGC death.

cAMP/Epac pathway mediates RGC damage in microbead-induced glaucoma

Acute glaucoma is caused by a rapid or sudden prominent increase of IOP because of halted aqueous outflow due to blockage of drainage canals, and prompt treatment is needed to avoid irreversible retinal neuronal damage (Ang and Ang, 2008; Weinreb et al., 2014). In contrast, chronic glaucoma (also known as primary open-angle glaucoma), the most prevalent form of glaucoma, is caused by decreased aqueous outflow due to the

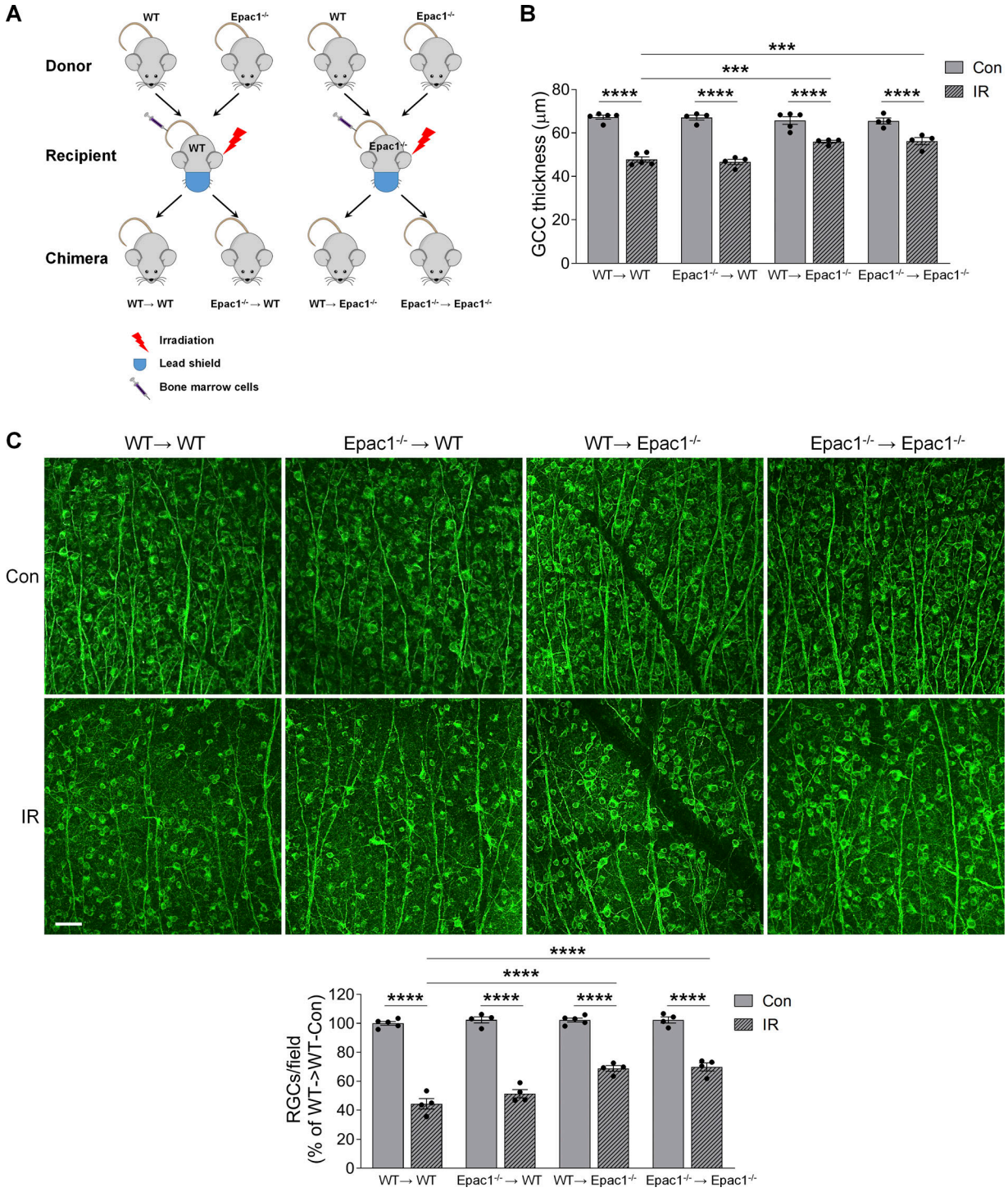

Figure 6. **Epac1 in resident retinal cells is responsible for neurodegeneration after IR injury.** Irradiated WT or *Epac1*$^{-/-}$ mice received BM transplant from WT or *Epac1*$^{-/-}$ mice respectively, and 6 wk later they were subjected to IR. **(A)** Schematic diagram showing different BM transplantation in WT (WT→WT and *Epac1*$^{-/-}$→WT) and *Epac1*$^{-/-}$ (WT→*Epac1*$^{-/-}$ and *Epac1*$^{-/-}$→*Epac1*$^{-/-}$) recipients. **(B)** Quantification of the thickness of GCC in different chimeric mice 7 d after IR. *n* = 4–5 mice. **(C)** Representative images of retinal flatmounts labeled with Tuj1 antibody (green) 7 d after IR. Scale bar: 50 µm. Bar graph represents the percentage of Tuj1-positive cells per field relative to control retinas from WT→WT mice. *n* = 4–5 mice; eight images were taken at the peripheral retina for each sample and calculated as average value. ***, P < 0.001; ****, P < 0.0001; one-way ANOVA. Error bars represent SEM.

slow clogging of the drainage canals, resulting in moderate but sustained IOP increase that leads to progressive degeneration of RGCs and their axons. To further address the pathologic role of Epac1 in glaucoma, we used a mouse microbead-induced glaucoma model that has been widely used to study RGC injury in glaucoma (Cone et al., 2010, 2012; Sappington et al., 2010; Yang et al., 2012a). In this model, polystyrene microbeads were injected intracamerally and accumulated in the iridocorneal

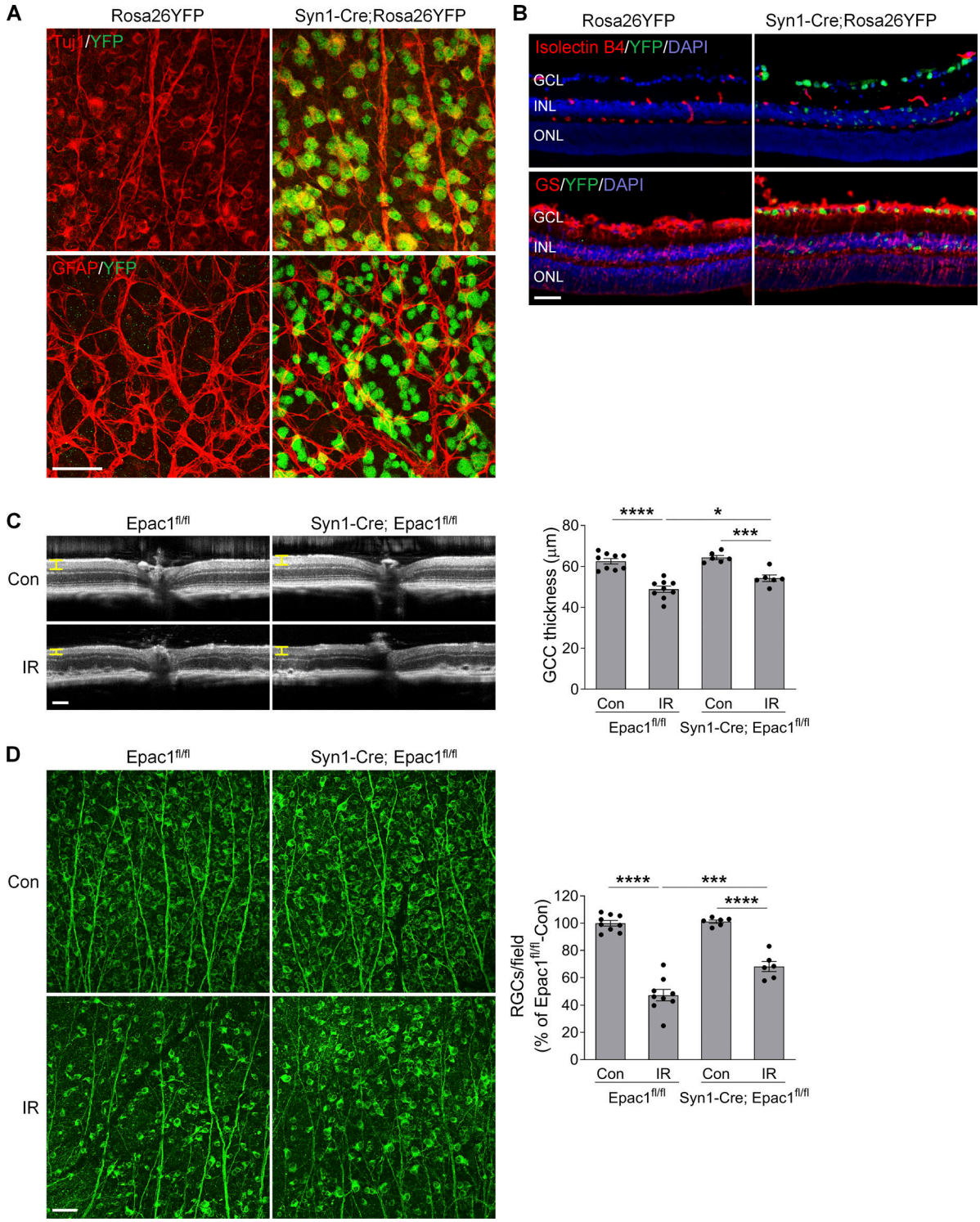

Figure 7. ***Epac1* deletion in neurons alleviates RGC death after IR injury. (A and B)** Syn1-Cre mice were crossed with Rosa26YFP reporter mice to generate Syn1-Cre; Rosa26YFP mice. Retinal flatmounts (A) or sections (B) were stained with antibodies against YFP (green) and different retinal cell markers (red). Tuj1 for RGCs; GFAP for astrocytes; isolectin B4 for vessels; and glutamine synthetase (GS) for glia (astrocytes and Müller cells). Blue, DAPI staining for nuclei. **(C)** OCT analysis in live *Epac1*$^{fl/fl}$ and Syn1-Cre; *Epac1*$^{fl/fl}$ mice (C57BL/6 background) for retinal thickness 7 d after IR. Yellow H lines indicate the thickness of GCC. Bar graph represents the thickness of GCC. *n* = 6–9 mice. Scale bar: 100 µm. **(D)** Representative images of retinal flatmounts labeled with Tuj1 antibody (green) in *Epac1*$^{fl/fl}$ and Syn1-Cre; *Epac1*$^{fl/fl}$ mice 7 d after IR. Scale bar: 50 µm. Bar graph represents the percentage of Tuj1-positive cells per field relative to *Epac1*$^{fl/fl}$ control. *n* = 6–9 mice; eight images were taken at the peripheral retina for each sample and calculated as average value. *, P < 0.05; ***, P < 0.001; ****, P < 0.0001; one-way ANOVA. Error bars represent SEM.

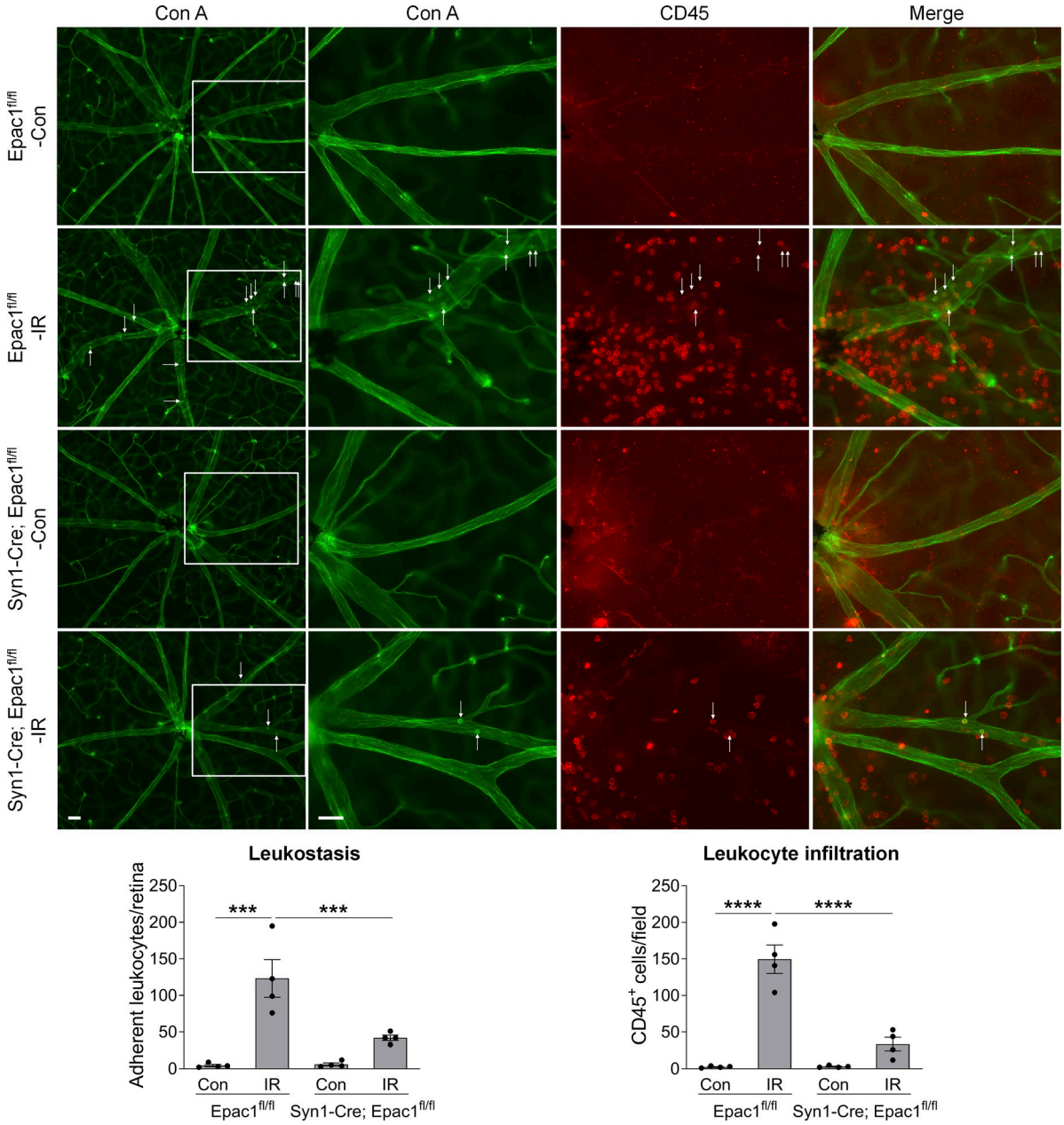

Figure 8. ***Epac1* deletion in neurons diminishes leukostasis in the retina after IR injury.** Representative images of leukostasis in the central retinas. *Epac1*$^{fl/fl}$ and Syn1-Cre; *Epac1*$^{fl/fl}$ mice were subjected to IR, and leukostasis assay was performed 24 h after IR. Green, Con A–labeled retinal vasculature and adherent leukocytes; red, CD45 immunostaining for leukocytes. Rectangles in the left rows of images are zoomed in, and arrows indicate stationary leukocytes adherent to the vascular endothelium. Bar graphs represent the number of leukocytes adherent to the retinal vasculature (Con A$^+$, CD45$^+$) per retina and infiltrated leukocytes (Con A$^-$, CD45$^+$) per field (four images were taken randomly for each eye and calculated as average value). *n* = 4 mice; ***, P < 0.001; ****, P < 0.0001; one-way ANOVA. Scale bar: 50 µm. Error bars represent SEM.

angle and Schlemm's canal (Fig. 10 A) and partially blocked the drainage of aqueous humor, resulting in a moderate but sustained increase in IOP similar to that in chronic glaucoma (Fig. 10 B). Consistent with the results from the IR model, cAMP accumulated in the cells of the GCL (Fig. 10 C), and Epac1 protein was markedly increased (Fig. 10, C and D) in glaucomatous retinas of WT mice 7 d after microbead injection compared with sham controls. A marked decrease in RGC number was observed in glaucomatous retinas of WT mice in comparison with control eyes 6 wk after microbead injection (Fig. 10 E). Although *Epac1*$^{-/-}$ mice had IOPs similar to those of WT mice (Fig. 10 B), *Epac1* deletion markedly attenuated RGC loss (Fig. 10 E). These results indicate that Epac1 plays a critical role in neurodegeneration during chronic glaucoma.

Discussion

Mechanisms of RGC injury in glaucoma remain to be elucidated. In the present study, we demonstrated that the activity and expression of Epac1 were increased in two experimental mouse

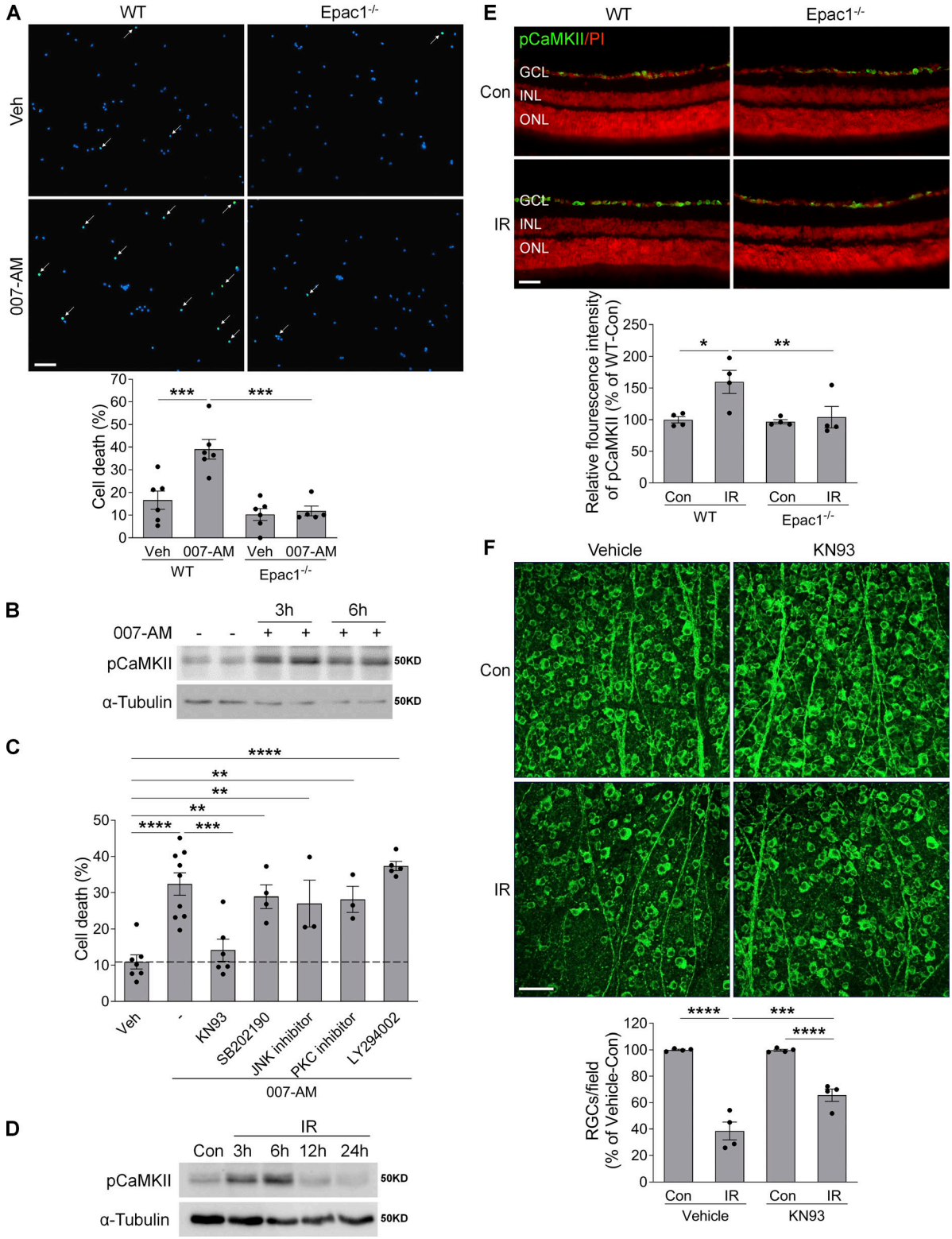

Figure 9. **Epac1 activation promotes RGC death through pCaMKII. (A)** Primary mouse RGCs isolated from WT and *Epac1*$^{-/-}$ pups were treated with 007-AM (10 µM) or vehicle for 18 h. Cell death was determined by TUNEL assay. *n* = 5–6; five images were taken randomly for each sample and calculated as average value. **(B)** The expression of pCaMKII in primary RGCs treated with 007-AM (10 µM). *n* = 3. **(C)** Primary RGCs isolated from WT pups were treated with 007-AM (10 µM) in the presence of different inhibitors for 18 h, and cell death was determined by TUNEL assay. *n* = 3–9; five images were taken randomly for each sample and calculated as average value. **(D)** The expression of pCaMKII in retinas at various time points after IR by Western blotting. **(E)** The expression of pCaMKII (green) in retinal sections from WT and *Epac1*$^{-/-}$ mice 3 h after IR. Red, PI staining. *n* = 4 mice. Immunostaining intensity was quantified from three independent observed areas of each retinal section. For each eye, data from three sections were averaged. **(F)** Representative images of retinal flatmounts labeled with Tuj1 antibody (green) 7 d after IR in vehicle or KN93-treated WT mice. Bar graph represents the percentage of Tuj1-positive cells per field relative to vehicle-treated control retinas. *n* = 4 mice; eight images were taken at the peripheral retina for each sample and calculated as average value. *, P < 0.05; **, P < 0.01; ***, P < 0.001; ****, P < 0.0001; one-way ANOVA. Scale bar: 50 µm. ONL, outer nuclear layer. Error bars represent SEM.

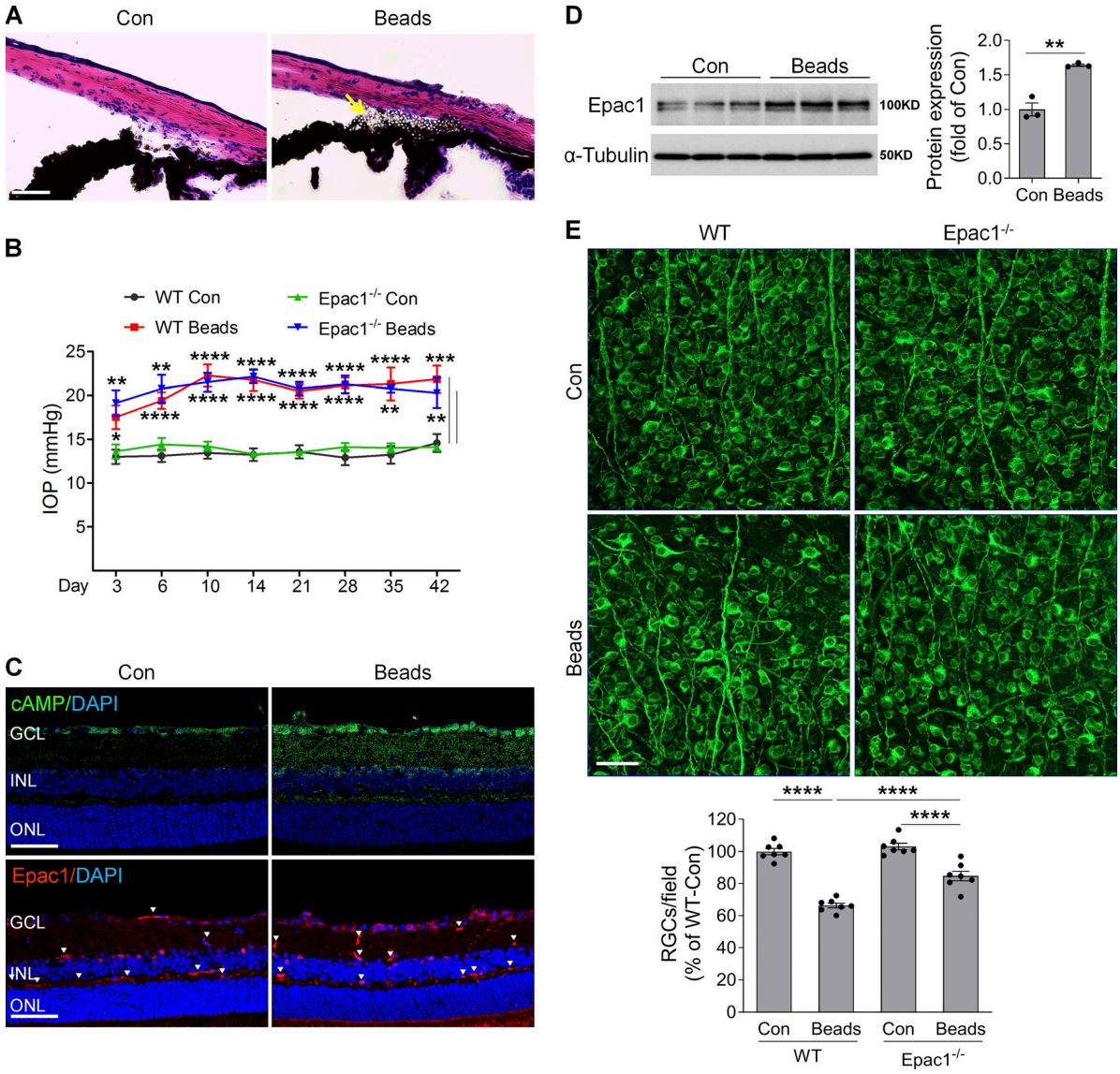

Figure 10. **cAMP/Epac1 mediates RGC injury in microbead-induced glaucoma.** WT and *Epac1*$^{-/-}$ mice at 2 mo of age were injected with microbeads into the anterior chamber to induce IOP. **(A)** Representative images show microbead distribution in the mouse anterior chamber following intracameral injection. **(B)** IOP elevation in WT and *Epac1*$^{-/-}$ mice at various time points following microbead injection. *n* = 8–10; *, P < 0.05; **, P < 0.01; ***, P < 0.001; ****, P < 0.0001; Student's *t* test for each time point. **(C)** The immunoactivity of cAMP (green, upper panel) and Epac1 (red, lower panel) in the retinal sections of WT mice 7 d after microbead injection. Blue, DAPI staining for nuclei. Arrowheads indicate nonspecific staining on vessels. *n* = 4 mice. **(D)** Epac1 protein expression in WT retinas 7 d after microbead injection. *n* = 3; two retinas were pooled for one sample. **, P < 0.01; Student's *t* test. **(E)** Retinal flatmounts from WT and *Epac1*$^{-/-}$ mice were labeled with Tuj1 antibody (green) 6 wk after microbead injection. *n* = 7 mice; eight images were taken at the peripheral retina for each sample and calculated as average value; ****, P < 0.0001; one-way ANOVA. Scale bar: 50 µm. ONL, outer nuclear layer. Error bars represent SEM.

models of ocular hypertension that have been used to study mechanisms of RGC injury and neuroprotection in glaucoma, and that deletion of *Epac1* prevented RGC loss and preserved its function. Moreover, by selectively deleting Epac1 in different cell types, we found that Epac1 expressed in RGCs played a key role in inducing RGC death in a process involved in the activation of CaMKII. Using Epac inhibitor ESI-09, our data further showed that pharmacologic blockade of Epac is beneficial and preserves RGCs after retinal injury. Given that RGC loss results in irreversible vision loss in glaucoma and that lowering IOP, the only proven therapeutic option to treat this disease, is not always effective to prevent visual loss in all glaucoma patients, pharmacologic interventions that can save RGCs and preserve vision are highly desired. Our study suggests that Epac1 is a novel target for neuroprotection in glaucoma and warrants further investigation of this pathway in glaucoma and evaluation of the effects of newly developed Epac inhibitors (Ye et al., 2015).

cAMP regulates many pathophysiological events, yet its role in retinal neuronal injury is less known. Since activation of protein kinase A prevents neuronal apoptosis by multiple mechanisms, including phosphorylation of GSK-3β, inhibition of the apoptotic activity of GSK-3β, and prevention of mitochondrial Ca^{2+} overload by phosphorylation of the mitochondrial

Na^+/Ca^{2+} exchanger (Kostic et al., 2015; Li et al., 2000), it is possible that increase in cAMP is an endogenous protective mechanism that prevents retinal neuronal injury. Nevertheless, it has been shown that blocking $A_{2A}R$ (Liu et al., 2016; Madeira et al., 2015, 2016), a Gs protein–coupled receptor that induces cAMP formation, or activating Gi protein–coupled receptors (e.g., SST2R or opioid receptors) that inhibit cAMP production (Abdul et al., 2013; Cervia et al., 2003; Husain et al., 2009; Kiagiadaki and Thermos, 2008), significantly prevents retinal neuronal injury, suggesting a damaging role of cAMP signaling in retinal neuropathy. This contradiction suggests that other molecules downstream of cAMP mediate its effect on neuronal injury. Our study indicates that Epac1 is one such mediator, since global or RGC-specific deletion of *Epac1* protects RGCs from high IOP–induced injury. This study is in line with previous work showing that activation of Epac leads to apoptosis in cortical neurons and *Epac1* deletion abolishes 3-nitropropionic acid–induced neuronal apoptosis (Suzuki et al., 2010). Interestingly, while we found that Epac1 plays a pathologic role in RGC injury, a recent study showed that deleting Epac1 in endothelial cells accelerated retinal neuronal injury and capillary degeneration after ischemic injury (Liu et al., 2018). This discrepancy suggests that Epac1 may exert different functions in different cell types. It is also important to point out that while mice with C57BL/6 background were used in this study, mice used in the aforementioned study were on mixed background (B6/129S). Therefore, the discrepancy could also be due to the different genetic backgrounds of mice used. While Epac activation in different cell types may exert diverse effects, its activation in neurons as well as in cardiomyocytes causes cell damage and leads to disease (Laudette et al., 2019; Okumura et al., 2014; Singhmar et al., 2016; Wang et al., 2013). A recent study further shows that Epac inhibition reverses mechanical allodynia and loss of intraepidermal nerve fibers in a mouse model of chemotherapy-induced peripheral neuropathy (Singhmar et al., 2018).

Infiltration of leukocytes to the injured eye accelerates retinal neuronal damage after ischemia (Ha et al., 2015, 2017). Since Epac1 is expressed in leukocytes (Lorenowicz et al., 2006; Scott et al., 2016) and Epac/Rap1 signaling promotes leukocyte migration and activation by enhancing monocyte adhesion and chemotaxis in a β1-integrin–dependent manner (Lorenowicz et al., 2006) and improves neutrophil phagocytosis (Scott et al., 2016), it is likely that deleting Epac1 in immune cells may attenuate retinal inflammation as well as neuronal damage. However, our study found that introducing *Epac1*$^{-/-}$ BM to WT mice (*Epac1*$^{-/-}$→WT) did not attenuate GCC thinning (the same as in WT→WT mice), indicating that Epac1 in immune cells had no effect on RGC survival after injury. In contrast, although both WT→*Epac1*$^{-/-}$ and WT→WT mice had WT leukocytes, the GCC of WT→*Epac1*$^{-/-}$ was thicker than that of WT→WT, indicating that deleting Epac1 in retinal cells attenuated RGC loss. Given that expression of Epac1 in glial and myeloid cells did not contribute to IOP-induced retinal pathology (Fig. S4 and Fig. S5), and that global deletion of *Epac1* or systemic treatment of Epac inhibitor prevented RGC damage, Epac1 activation in retinal neurons may have a dominant role in driving retinal neuropathy in glaucoma. Moreover, a significant reduction of leukocyte recruitment in *Epac1*$^{-/-}$ and *Epac1*$^{RGC\text{-}KO}$ mice suggests that activation of Epac1 in neurons may have an impact on vascular alterations via the cross-talk between neurons and vessels. This notion is further supported by our data that *Epac1* deletion substantially attenuated IR-induced increase in retinal vascular leakage, although activation of Epac is known to promote the integrity of endothelial cell junctions. During retinal ischemic injury, stressed and dysfunctional neurons may send signals to vasculature to regulate its response, including causing vascular inflammation and barrier breakdown. Consequently, deletion of *Epac1* not only attenuated retinal neuronal injury but also reduced vascular changes in the IR model.

Many kinases, including CaMKII, JNK, p38MAPK, protein kinase C, and AKT, are involved in the pathophysiological events induced by Epac activation (Breckler et al., 2011; Robichaux and Cheng, 2018). Our study demonstrates that CaMKII was rapidly activated after IOP-induced retinal ischemia in an Epac1-dependent manner and that blocking CaMKII markedly attenuated RGC death in vivo and in vitro, highlighting the critical involvement of CaMKII in Epac1-induced retinal neuronal injury. Epac-mediated CaMKII activation has been well documented in the literature. It is known that upon activation by Epac, Rap binds to and activates phospholipase C ε, resulting in hydrolysis of phosphatidylinositol 4,5-bisphosphate, formation of inositol triphosphate, and subsequent release of Ca^{2+} from intracellular stores. Elevated intracellular Ca^{2+} leads to the activation of CaMKII, which further autophosphorylates at threonine 286, causing enhanced and prolonged kinase activity (Oestreich et al., 2009). In cardiac myocytes and skeletal muscle cells, the Epac/CaMKII pathway regulates Ca^{2+} homeostasis, excitation–transcription coupling, and gene expression and is involved in cardiac hypertrophy, arrhythmia, and skeletal hypertrophy (Liu and Schneider, 2013; Métrich et al., 2008; Ohnuki et al., 2014; Pereira et al., 2007, 2015). Nevertheless, it is largely unknown whether the Epac/CaMKII pathway regulates neuronal function or death, although it is well appreciated that CaMKII can induce cell apoptosis and necroptosis via JNK-mediated Fas/FasL expression, mitochondria-initiated intrinsic apoptotic pathway, and triggering the opening of the mitochondrial permeability transition pore (Goebel, 2009; Jiang et al., 2014; Joiner et al., 2012; Liu et al., 2013; Timmins et al., 2009; Toledo et al., 2014; Zhang et al., 2016). Our work represents the first to link the Epac/CaMKII pathway to neuronal damage, particularly in the context of experimental glaucoma. This study, together with studies showing that CaMKII mediates retinal neuronal and vascular injury in diabetic retinopathy and is involved in growth factor–induced retinal and choroidal neovascularization (Ashraf et al., 2019; Kim et al., 2010, 2011; Li et al., 2015), highlights the potential value of Epac1/CaMKII inhibition in treating a variety of retinopathies. Of note, an interesting quality of Epac signaling has been compartmentalization of the protein. The formation of a β-arrestin–CaMKII–Epac1 complex allows its recruitment to the plasma membrane, where it permits activation of Epac1 by β1-adrenergic receptor stimulation–induced cAMP and subsequent CaMKII activation (Mangmool et al., 2010). Meanwhile, perinuclear Epac1

localization can induce activation of calcineurin/nuclear factor of activated T-cells and CaMKII/histone deacetylase hypertrophic pathways (Pereira et al., 2015). Future studies will examine whether Epac1 in RGCs assumes a perinuclear location or is more associated with microtubules in order to better understand Epac1-induced RGC death.

In summary, using genetic and pharmacologic approaches, we demonstrate that blockade of Epac1 is neuroprotective in mouse models of ocular hypertension. On the other hand, activation of Epac1 induces RGC death via CaMKII. Since Epac1 is also expressed in neurons in the brain, and its level is increased in Alzheimer's disease, further investigation of Epac1 in neuronal injury in other neurodegenerative models such as traumatic optic neuropathy, stroke, and Alzheimer's disease may address whether activation of Epac1 is a unified mechanism of neuronal injury or is a mechanism applicable only to glaucoma.

Materials and methods

Animals

Epac1$^{flox/flox}$ (stock no. 018389), Syn1-Cre (stock no. 003966), GFAP-Cre (stock no. 024098), LysM-Cre (stock no. 004781), and Rosa26YFP (stock no. 006148) mice were purchased from the Jackson Laboratory. C57BL/6 mice were originally obtained from the Jackson Laboratory and subsequently bred in the animal care facility at the University of Texas Medical Branch. *Epac1*$^{-/-}$ mice were kindly provided by Dr. Ju Chen (University of California, San Diego, San Diego, CA) and described previously (Yan et al., 2013). All transgenic mice were backcrossed into C57BL/6 background before using to generate tissue-specific knockout mice. Mice were maintained on a 12:12 light/dark cycle with food and water available ad libitum. All experimental procedures and use of animals were approved by the Institutional Animal Care and Use Committee of the University of Texas Medical Branch.

Mouse model of retinal IR

Mice (8–10 wk old) were anesthetized by i.p. injection of a mixture of 100 mg/kg ketamine hydrochloride and 10 mg/kg xylazine hydrochloride. After 0.5% proparacaine hydrochloride was applied topically and the pupils were dilated with 1% tropicamide and 2.5% phenylephrine, the anterior chamber of the right eye was cannulated with a 30-gauge infusion needle connected to a reservoir of sterile saline, which was elevated to maintain the IOP at 110 mm Hg for 45 min. The contralateral left eye without elevating the pressure served as control. The animal's temperature was maintained using a heat pad. Eyes or retinas were collected at the indicated time points after IR. ESI-09 (20 mg/kg; SML0814; Sigma-Aldrich), KN-93 (2.5 mg/kg; 422708; Sigma-Aldrich), or vehicle (PBS containing 10% Tween 80 and 20% ethanol) was i.p. injected 6 h before IR was performed and once a day thereafter for 6 d.

Microbead-induced glaucoma model

Microbead-induced glaucoma was induced using a modified protocol based on previous publications (Sappington et al., 2010; Yang et al., 2012a). Mice (8–10 wk old) were anesthetized by i.p. injection of a mixture of 100 mg/kg ketamine hydrochloride and 10 mg/kg xylazine hydrochloride. After 0.5% proparacaine hydrochloride was applied topically and the pupils were dilated with 1% tropicamide and 2.5% phenylephrine, the cornea was gently punctured using a 30-gauge needle. Next, 2 µl of 1-µm-diameter polystyrene microbead suspension (containing 3.0 × 10^7 beads) followed by an air bubble, 2 µl of 6-µm-diameter polystyrene microbead suspension (containing 6.3 × 10^6 beads, Polysciences), and 1 µl of PBS containing 30% Healon was injected into the anterior chamber using a 32-gauge needle (Hamilton Company) connected to a syringe (Hamilton Company), which induced moderate elevation of IOP for ≥6 wk. An equivalent volume of PBS was injected into the contralateral eyes to serve as control (sham). IOP was measured using a tonometer (TonoLab, Colonial Medical Supply) 3 d after injection thereafter until 6 wk after injection between 3 p.m. and 5 p.m. to minimize diurnal variability.

BM transplantation

BM transplantation was performed as described previously (Ha et al., 2017). In brief, recipient WT or *Epac1*$^{-/-}$ mice at 6 wk of age were irradiated at a dose of 8.5 Gy (850 rads) using a Gammacell 40 irradiator (MDS Nordion), with a lead shield used to protect the head and eyes. BM cell suspensions from donor WT or *Epac1*$^{-/-}$ mice were prepared by flushing femurs and tibias with PBS using a 23-gauge needle. Following washing, cells were counted and resuspended in Dulbecco's PBS without Ca^{2+}/Mg^{2+} before injection. Within 24 h after irradiation, recipient mice were reconstituted with 200 µl cell suspension containing 0.7–1.0 × 10^7 cells via tail vein injection. 6 wk later, chimeric mice were subjected to IR.

High-resolution en face OCT

7 d after IR, mice were anesthetized with an i.p. injection of a mixture of 100 mg/kg ketamine and 10 mg/kg xylazine. After pupils were dilated with tropicamide and phenylephrine, mice were positioned on the imaging platform for radial and annular scans with a Spectral Domain Ophthalmical Imaging System (Envisu R2200, Bioptigen; Ha et al., 2018; Liu et al., 2017; Yang et al., 2012a). A representative radial B-scan from the same location of the retina was selected for illustrative purposes only. For quantification, annular scans consisting of 1,000 A-scans × 100 B-scans covering a donut-shaped area centered at the optic nerve disc were performed. The inner and outer radii of the donut-shaped area were 200 and 700 µm from the center of the optic nerve disc, respectively, in order to remove variance of optic nerve head measurement. OCT depth thickness report and analysis were generated from Bioptigen's automated segmentation algorithm developed for the murine eye. The thickness of each retinal layer presented in the report for each eye was an average of 100,000 measurements (A-scans) in the donut-shaped area, which accurately measured retinal thickness and excluded the necessity to register and quantify the same anatomic landmark between different animals. The GCC is the sum of the three innermost layers: the nerve fiber layer, the GCL, and the inner plexiform layer (Ha et al., 2018; Liu et al., 2017; Yang et al., 2012a).

Histologic examination

The eyes were embedded in optimal cutting temperature compound, frozen, and cryosectioned to a thickness of 10 µm. Sections were then stained with H&E. The thickness of total retina and individual retinal layers was measured with LAS EZ software (Leica).

Leukostasis

Retinal leukostasis assay, which allows labeling of leukocytes adherent to the retinal endothelium, was performed as described previously (Liu et al., 2019; Rojas et al., 2010). This assay has been widely used to study retinal vascular inflammation in mouse models of retinopathies (Al-Shabrawey et al., 2008; Chen et al., 2013; Gubitosi-Klug et al., 2008; Liu et al., 2019; Moore et al., 2003; Rojas et al., 2010). Briefly, 24 h after IR procedure, mice were deeply anesthetized by i.p. injection of a mixture of 100 mg/kg ketamine hydrochloride and 10 mg/kg xylazine hydrochloride. After the chest cavity was carefully opened, a 20-gauge perfusion cannula was introduced into the aorta, and mice were perfused with 10 ml PBS through the left ventricle of the heart to remove nonadherent blood cells. Next, 10 ml FITC-conjugated Con A lectin (40 µg/ml in PBS, pH 7.4; RL-1002, Vector Laboratories) was perfused to label the adherent leukocytes and vasculature, followed by 10 ml PBS perfusion to remove the residual unbound Con A. After eyeballs were collected and fixed with 4% paraformaldehyde (PFA) overnight, retinas were dissected and stained with anti-CD45 antibody (1:400, 550539, BD Biosciences). Leukocytes inside the blood vessels (leukostasis) are Con A^+, $CD45^+$ (green and red fluorescence), while leukocytes outside the blood vessels (leukocytes infiltrated into the retina) are Con A^-, $CD45^+$ (only red fluorescence). The total number of the adherent leukocytes per retina and leukocytes infiltrated into the retina per field were counted.

Permeability assay

24 h after IR, mice were anesthetized and injected with FITC-BSA (Sigma-Aldrich, 100 mg/kg body weight) through the tail vein. 1 h after injection, whole blood was obtained from the right ventricle and centrifuged at 2,000 *g* for 15 min for plasma, which was diluted 100 times with 1× Passive lysis buffer (Promega). Next, mice were perfused via the left ventricle with PBS to remove intravascular blood. The whole retinas were isolated from eyeballs carefully to avoid contamination of aqueous humor, homogenized with 1× Passive lysis buffer, and centrifuged at 16,600 *g* for 15 min. Subsequently, fluorescence intensity in the supernatant from the retinal homogenate and diluted plasma were measured by Synergy H1 Hybrid Multi-Mode Reader (Biotek) with excitation at 485 nm and emission at 528 nm. Retinal homogenate and diluted plasma from mice without FITC-BSA injection were used as blank. Finally, fluorescence intensity in the retina was adjusted by retinal weight and the fluorescence of the plasma and normalized to noninjured retinas from WT mice.

Immunostaining of retinal whole mounts and counting of RGCs

The eyes were fixed in 4% PFA at 4°C overnight. Next, retinas were dissected from the choroid and sclera, washed with PBS, blocked, and permeabilized with PBS containing 5% normal goat serum and 0.3% Triton-X-100 for 3 h. Subsequently, retinas were incubated with antibodies against Iba1 (1:200, 019-19741, Wako), Tuj1 (1:400, 801202, BioLegend), YFP (1:1,000, ab13970, Abcam), or GFAP (1:200, Z033401-2, Dako) at 4°C overnight. After washing, retinas were incubated with Alexa Fluor 488– or 594–conjugated secondary antibodies (1:400, Life Technologies) at 4°C for 4 h. Finally, retinas were mounted for confocal microscopy (LSM 510 Meta, Carl Zeiss). To count RGCs, eight nonoverlapping images were taken at the peripheral region of each retinal flatmount stained with Tuj1 antibody. RGCs were manually counted, and the average value was calculated for each sample.

Immunofluorescence

The eyes were fixed with 4% PFA in 0.1 M phosphate buffer for 60 min, equilibrated in 30% sucrose overnight, embedded in optimal cutting temperature compound, frozen, and cryosectioned to a thickness of 10 µm. Sections were then post-fixed with 4% PFA in PBS for 10 min, rinsed with PBS, permeabilized with PBS containing 0.1% Triton X-100 for 15 min at room temperature, and blocked with PowerBlock (Biogenx) for 1 h. Subsequently, sections were probed with isolectin B4 or primary antibodies against cAMP (1:400, 07-1497, EMD Millipore), Epac1 (1:250, SC28366, Santa Cruz Biotechnology), glutamine synthetase (1:1,000, AB302, EMD Millipore), YFP (1:2,000, ab13970, Abcam), pRIP3 (1:2,000, ab205421, Abcam), or pCaMKII (1:1,000, ab32678, Abcam). After three washes with PBS, sections were incubated with Alexa Fluor 488– or 594–conjugated secondary antibodies (1:1,000, Life Technologies), mounted with medium containing DAPI (Abcam), and imaged with epifluorescence microscopy or confocal microscopy (Carl Zeiss).

Isolation of primary RGCs

Primary RGCs were isolated according to the two-step immunopanning protocol. In brief, retinas were collected from WT mouse pups at postnatal day 4–5 and dissociated in a papain solution (15 U/ml) at 37°C for 30 min. Next, dissociated retina cell suspensions were incubated with anti-macrophage antiserum (Accurate Chemical) to remove macrophages and microglial cells. Subsequently, nonadherent cells were incubated with mouse Thy-1.2 antibody (BD Biosciences) to purify RGCs, which were then released by incubation with trypsin solution and quenched by the addition of 30% FBS and 1 mg/ml of ovomucoid trypsin inhibitor in Neurobasal medium. After counting, RGCs were plated on poly-D-lysine and laminin–coated plates. For TUNEL assay, RGCs were seeded in a 24-well plate at a density of 1.8×10^5 cells/well and treated with 007-AM (10 µM) in the presence or absence of kinase inhibitors for 18 h, the optimal time required for peak DNA fragmentation by both extrinsic and intrinsic apoptosis inducers in primary RGCs (Dun et al., 2007; Ha et al., 2011, 2012). After treatment, RGCs were fixed and subjected to TUNEL to detect cell death. For Western blot assay, RGCs were seeded in a six-well plate at a density of 1.8×10^6 cells/well and treated with 007-AM (10 µM) for 3 and 6 h the next day.

TUNEL

TUNEL was performed using ApopTag Fluorescein In situ Apoptosis Detection Kit (EMD Millipore) according to the manufacturer's instructions. Retinal sections or RGCs were prepared as described above and counterstained with DAPI to label nuclei. After staining, images were taken by epifluorescence microscopy, and TUNEL-positive cells were counted. The percentage of apoptotic RGCs in vitro was calculated as the ratio of TUNEL-positive cells to DAPI-positive cells per field of view.

PI uptake

PI uptake assay was performed to label necrotic cells as described previously (Liu et al., 2019; Shosha et al., 2016; Unal Cevik and Dalkara, 2003). Briefly, mice were given i.p. administration of 5 mg/kg PI (Thermo Fisher Scientific) 9 h after IR. Then, eyeballs were harvested for cryosectioning 3 h after PI injection. The total number of PI-positive cells per section was counted under fluorescence microscopy.

Active Rap1 pull-down

GTP-bound Rap1 was detected using a Rap1 Activation Assay Kit (EMD Millipore) according to the manufacturer's instructions. Briefly, retinas were lysed in lysis buffer supplemented with protease inhibitor. Retinal lysates were then incubated with GST-RalGDS-RBD fusion protein and glutathione resin beads for 1 h at 4°C. Proteins collected on the beads were subjected to SDS-PAGE, followed by immunoblotting with anti-Rap1 antibody.

Western blot

Retinas were homogenized using an electric homogenizer in radioimmunoprecipitation assay lysis buffer (50 mM Tris-HCl, pH 7.4, 150 mM NaCl, 0.25% deoxycholic acid, 1% NP-40, and 1 mM EDTA) with Complete Protease and Phosphatase Inhibitors (Roche Applied Science). Protein concentration was quantified using the Bradford assay (Bio-Rad) according to the manufacturer's instructions. Protein sample was diluted in loading buffer and heated at 95°C for 10 min. Equivalent amounts of protein were electrophoresed on 10% or 12% SDS-polyacrylamide gels and transferred to polyvinylidene fluoride membranes. After the membranes were blocked with 5% nonfat dry milk for 1 h at room temperature, they were incubated overnight at 4°C with primary antibodies against Epac1 (1:500, 4155, Cell Signaling Technology) and pCaMKII (1:2,000, ab32678, Abcam). After three washes with Tris buffered saline and Tween 20, the membranes were incubated for 1 h at room temperature with HRP-conjugated secondary antibody (1:2,000; Amersham Biosciences). After washing, proteins were detected by enhanced chemiluminescence (Pierce) using either x-ray film or the Bio-Rad ChemiDoc XRS+. For internal control, membrane was probed for α-Tubulin mouse monoclonal antibody (Sigma-Aldrich). The band intensities were quantified using ImageJ (National Institutes of Health) and normalized against α-Tubulin. Relative changes in protein expression were calculated in relation to control retinas and expressed as x-fold change.

Real-time quantitative RT-PCR

Total RNA was isolated from the retina using RNAqueous-4PCR kit (Life Technologies) according to the manufacturer's instructions. After quantification with NanoDrop, RNA was converted to cDNA using High Capacity cDNA Reverse Transcription Kit (Life Technologies). Quantitative PCR was performed with SYBR Green Master Mix (Applied Biosystems) using a StepOnePlus PCR system (Life Technologies). Primer sequences were as follows: Epac1 For (forward), 5′-AATGGC TGTGGGAACGTATCTC-3′ Epac1 Rev (reverse), 5′-CCTGGTTAG GGAGCCAAACA-3′; Epac2 For, 5′-TGCAAACACTGCCAGAAC AGT-3′, and Epac2 Rev, 5′-GAGCGGCATCCGGATTG-3′; and Hprt For, 5′-GAAAGACTTGCTCGAGATGTCATG-3′, and Hprt Rev, 5′-CACACAGAGGGCCACAATGT-3′. The fold difference was calculated by the ΔΔCT method using Hprt as the internal control.

Dark-adapted ERG analysis

ERG analysis was performed during daytime as described previously (Ha et al., 2017, 2018; Liu et al., 2019). In brief, 14 d after IR, mice were dark-adapted overnight, anesthetized, and kept at a constant body temperature of 37°C on a self-heating platform. After dilation of the pupil with a mixture of atropine and phenylephrine and lubricating the cornea with Celluvisc, gold ring electrodes were placed on the surface of the cornea. Next, ERG responses were measured using the Espion system (Diagnosys). pSTRs were recorded in response to a series of white flashes with intensities ranging from −4.3 to −3.2 log cd · s/m^2. The a-wave amplitude is measured from baseline to the trough of a-wave. The b-wave amplitude is generally measured from the trough of a-wave to the peak of b-wave.

Statistics

Data were presented as mean ± SEM and analyzed by Student's *t* test or one-way ANOVA followed by Newman-Keuls post hoc test. Statistical analysis was conducted using Prism (GraphPad Software). A P value <0.05 was considered statistically significant.

Online supplemental material

Fig. S1 shows activation of Epac downstream targets (AKT and ERK) after ischemia and characterization of the retina of *Epac1*$^{-/-}$ mice. Fig. S2 shows *Epac1* deletion decreases leukostasis in the peripheral retina after IR injury. Fig. S3 shows that *Epac1* deletion prevents RGC loss 14 d after IR. Fig. S4 shows that *Epac1* deletion in myeloid cells does not affect RGC death after IR. Fig. S5 shows that *Epac1* deletion in astrocytes does not affect RGC death after IR.

Acknowledgments

We thank Dr. Ju Chen (University of California, San Diego, San Diego, CA) for *Epac1*$^{-/-}$ mice.

This work was supported in part by National Institutes of Health grant EY022694 and the Retina Research Foundation to W. Zhang, American Heart Association 17SDG33630151 to H. Liu, and National Institutes of Health grant GM122536 to X. Cheng.

Author contributions: W. Liu, Y. Ha, F. Xia, H. Liu, and W. Zhang designed the experiments. W. Liu, Y. Ha, F. Xia, S. Zhu, Y. Li, S. Shi, and H. Liu performed the experiments. W. Liu, Y. Ha, F. Xia, S. Zhu, Y. Li, S. Shi, H. Liu, and W. Zhang analyzed the data. F.C. Mei and X. Cheng provided key reagents. W. Liu, Y. Ha, F. Xia, K. Merkley, G. Vizzeri, M. Motamedi, X. Cheng, H. Liu, and W. Zhang wrote the manuscript.

Disclosures: The authors declare no competing interests exist.

Submitted: 23 May 2019
Revised: 6 September 2019
Accepted: 26 November 2019

References

Abdul, Y., N. Akhter, and S. Husain. 2013. Delta-opioid agonist SNC-121 protects retinal ganglion cell function in a chronic ocular hypertensive rat model. *Invest. Ophthalmol. Vis. Sci.* 54:1816–1828. https://doi.org/10.1167/iovs.12-10741

Al-Shabrawey, M., M. Rojas, T. Sanders, A. Behzadian, A. El-Remessy, M. Bartoli, A.K. Parpia, G. Liou, and R.B. Caldwell. 2008. Role of NADPH oxidase in retinal vascular inflammation. *Invest. Ophthalmol. Vis. Sci.* 49: 3239–3244. https://doi.org/10.1167/iovs.08-1755

Ang, L.P., and L.P. Ang. 2008. Current understanding of the treatment and outcome of acute primary angle-closure glaucoma: an Asian perspective. *Ann. Acad. Med. Singapore.* 37:210–215.

Ashraf, S., S. Bell, C. O'Leary, P. Canning, I. Micu, J.A. Fernandez, M. O'Hare, P. Barabas, H. McCauley, D.P. Brazil, et al. 2019. CAMKII as a therapeutic target for growth factor-induced retinal and choroidal neovascularization. *JCI Insight.* 4:122442.

Breckler, M., M. Berthouze, A.C. Laurent, B. Crozatier, E. Morel, and F. Lezoualc'h. 2011. Rap-linked cAMP signaling Epac proteins: compartmentation, functioning and disease implications. *Cell. Signal.* 23: 1257–1266. https://doi.org/10.1016/j.cellsig.2011.03.007

Cai, R., W. Xue, S. Liu, R.B. Petersen, K. Huang, and L. Zheng. 2015. Overexpression of glyceraldehyde 3-phosphate dehydrogenase prevents neurovascular degeneration after retinal injury. *FASEB J.* 29:2749–2758. https://doi.org/10.1096/fj.14-265801

Cervia, D., D. Fehlmann, and D. Hoyer. 2003. Native somatostatin sst2 and sst5 receptors functionally coupled to Gi/o-protein, but not to the serum response element in AtT-20 mouse tumour corticotrophs. *Naunyn Schmiedebergs Arch. Pharmacol.* 367:578–587. https://doi.org/10.1007/s00210-003-0752-1

Chen, H., C. Wild, X. Zhou, N. Ye, X. Cheng, and J. Zhou. 2014. Recent advances in the discovery of small molecules targeting exchange proteins directly activated by cAMP (EPAC). *J. Med. Chem.* 57:3651–3665. https://doi.org/10.1021/jm401425e

Chen, H., K.S. Cho, T.H.K. Vu, C.H. Shen, M. Kaur, G. Chen, R. Mathew, M.L. McHam, A. Fazelat, K. Lashkari, et al. 2018. Commensal microflora-induced T cell responses mediate progressive neurodegeneration in glaucoma. *Nat. Commun.* 9:3209. https://doi.org/10.1038/s41467-018-05681-9

Chen, Y., Y. Hu, M. Lin, A.J. Jenkins, A.C. Keech, R. Mott, T.J. Lyons, and J.X. Ma. 2013. Therapeutic effects of PPARα agonists on diabetic retinopathy in type 1 diabetes models. *Diabetes.* 62:261–272. https://doi.org/10.2337/db11-0413

Cheng, X., Z. Ji, T. Tsalkova, and F. Mei. 2008. Epac and PKA: a tale of two intracellular cAMP receptors. *Acta Biochim. Biophys. Sin. (Shanghai).* 40: 651–662. https://doi.org/10.1111/j.1745-7270.2008.00438.x

Chi, W., F. Li, H. Chen, Y. Wang, Y. Zhu, X. Yang, J. Zhu, F. Wu, H. Ouyang, J. Ge, et al. 2014. Caspase-8 promotes NLRP1/NLRP3 inflammasome activation and IL-1β production in acute glaucoma. *Proc. Natl. Acad. Sci. USA.* 111:11181–11186. https://doi.org/10.1073/pnas.1402819111

Clausen, B.E., C. Burkhardt, W. Reith, R. Renkawitz, and I. Förster. 1999. Conditional gene targeting in macrophages and granulocytes using LysMcre mice. *Transgenic Res.* 8:265–277. https://doi.org/10.1023/A:1008942828960

Cone, F.E., S.E. Gelman, J.L. Son, M.E. Pease, and H.A. Quigley. 2010. Differential susceptibility to experimental glaucoma among 3 mouse strains using bead and viscoelastic injection. *Exp. Eye Res.* 91:415–424. https://doi.org/10.1016/j.exer.2010.06.018

Cone, F.E., M.R. Steinhart, E.N. Oglesby, G. Kalesnykas, M.E. Pease, and H.A. Quigley. 2012. The effects of anesthesia, mouse strain and age on intraocular pressure and an improved murine model of experimental glaucoma. *Exp. Eye Res.* 99:27–35. https://doi.org/10.1016/j.exer.2012.04.006

Curry, F.E., T. Taxt, C.B. Rygh, T. Pavlin, R. Bjønrstad, S.O. Døskeland, and R.K. Reed. 2019. Epac1$^{-/-}$ mice have elevated baseline permeability and do not respond to histamine as measured with dynamic contrast-enhanced magnetic resonance imaging with contrast agents of different molecular weights. *Acta Physiol. (Oxf.).* 225:e13199. https://doi.org/10.1111/apha.13199

de Rooij, J., F.J. Zwartkruis, M.H. Verheijen, R.H. Cool, S.M. Nijman, A. Wittinghofer, and J.L. Bos. 1998. Epac is a Rap1 guanine-nucleotide-exchange factor directly activated by cyclic AMP. *Nature.* 396:474–477. https://doi.org/10.1038/24884

Do, Y.J., J.W. Sul, K.H. Jang, N.S. Kang, Y.H. Kim, Y.G. Kim, and E. Kim. 2017. A novel RIPK1 inhibitor that prevents retinal degeneration in a rat glaucoma model. *Exp. Cell Res.* 359:30–38. https://doi.org/10.1016/j.yexcr.2017.08.012

Dun, Y., M. Thangaraju, P. Prasad, V. Ganapathy, and S.B. Smith. 2007. Prevention of excitotoxicity in primary retinal ganglion cells by (+)-pentazocine, a sigma receptor-1 specific ligand. *Invest. Ophthalmol. Vis. Sci.* 48:4785–4794. https://doi.org/10.1167/iovs.07-0343

Dvoriantchikova, G., A. Degterev, and D. Ivanov. 2014. Retinal ganglion cell (RGC) programmed necrosis contributes to ischemia-reperfusion-induced retinal damage. *Exp. Eye Res.* 123:1–7. https://doi.org/10.1016/j.exer.2014.04.009

Goebel, D.J. 2009. Selective blockade of CaMKII-alpha inhibits NMDA-induced caspase-3-dependent cell death but does not arrest PARP-1 activation or loss of plasma membrane selectivity in rat retinal neurons. *Brain Res.* 1256:190–204. https://doi.org/10.1016/j.brainres.2008.12.051

Gubitosi-Klug, R.A., R. Talahalli, Y. Du, J.L. Nadler, and T.S. Kern. 2008. 5-Lipoxygenase, but not 12/15-lipoxygenase, contributes to degeneration of retinal capillaries in a mouse model of diabetic retinopathy. *Diabetes.* 57:1387–1393. https://doi.org/10.2337/db07-1217

Ha, Y., Y. Dun, M. Thangaraju, J. Duplantier, Z. Dong, K. Liu, V. Ganapathy, and S.B. Smith. 2011. Sigma receptor 1 modulates endoplasmic reticulum stress in retinal neurons. *Invest. Ophthalmol. Vis. Sci.* 52:527–540. https://doi.org/10.1167/iovs.10-5731

Ha, Y., W. Liu, H. Liu, S. Zhu, F. Xia, J.E. Gerson, N.A. Azhar, R.G. Tilton, M. Motamedi, R. Kayed, and W. Zhang. 2018. AAV2-mediated GRP78 Transfer Alleviates Retinal Neuronal Injury by Downregulating ER Stress and Tau Oligomer Formation. *Invest. Ophthalmol. Vis. Sci.* 59: 4670–4682. https://doi.org/10.1167/iovs.18-24427

Ha, Y., H. Liu, Z. Xu, H. Yokota, S.P. Narayanan, T. Lemtalsi, S.B. Smith, R.W. Caldwell, R.B. Caldwell, and W. Zhang. 2015. Endoplasmic reticulum stress-regulated CXCR3 pathway mediates inflammation and neuronal injury in acute glaucoma. *Cell Death Dis.* 6:e1900. https://doi.org/10.1038/cddis.2015.281

Ha, Y., H. Liu, S. Zhu, P. Yi, W. Liu, J. Nathanson, R. Kayed, B. Loucas, J. Sun, L.J. Frishman, et al. 2017. Critical Role of the CXCL10/C-X-C Chemokine Receptor 3 Axis in Promoting Leukocyte Recruitment and Neuronal Injury during Traumatic Optic Neuropathy Induced by Optic Nerve Crush. *Am. J. Pathol.* 187:352–365. https://doi.org/10.1016/j.ajpath.2016.10.009

Ha, Y., A. Saul, A. Tawfik, E.P. Zorrilla, V. Ganapathy, and S.B. Smith. 2012. Diabetes accelerates retinal ganglion cell dysfunction in mice lacking sigma receptor 1. *Mol. Vis.* 18:2860–2870.

Haas, C.A., L.J. DeGennaro, M. Müller, and H. Holländer. 1990. Synapsin I expression in the rat retina during postnatal development. *Exp. Brain Res.* 82:25–32. https://doi.org/10.1007/BF00230834

Hartsock, M.J., H. Cho, L. Wu, W.J. Chen, J. Gong, and E.J. Duh. 2016. A Mouse Model of Retinal Ischemia-Reperfusion Injury Through Elevation of Intraocular Pressure. *J. Vis. Exp.* (113):54065. https://doi.org/10.3791/54065

Husain, S., D.E. Potter, and C.E. Crosson. 2009. Opioid receptor-activation: retina protected from ischemic injury. *Invest. Ophthalmol. Vis. Sci.* 50: 3853–3859. https://doi.org/10.1167/iovs.08-2907

Jiang, G., H. Wu, Y. Hu, J. Li, and Q. Li. 2014. Gastrodin inhibits glutamate-induced apoptosis of PC12 cells via inhibition of CaMKII/ASK-1/p38 MAPK/p53 signaling cascade. *Cell. Mol. Neurobiol.* 34:591–602. https://doi.org/10.1007/s10571-014-0043-z

Joiner, M.L., O.M. Koval, J. Li, B.J. He, C. Allamargot, Z. Gao, E.D. Luczak, D.D. Hall, B.D. Fink, B. Chen, et al. 2012. CaMKII determines mitochondrial stress responses in heart. *Nature.* 491:269–273. https://doi.org/10.1038/nature11444

Kawasaki, H., G.M. Springett, N. Mochizuki, S. Toki, M. Nakaya, M. Matsuda, D.E. Housman, and A.M. Graybiel. 1998. A family of cAMP-binding proteins that directly activate Rap1. *Science.* 282:2275–2279. https://doi.org/10.1126/science.282.5397.2275

Kiagiadaki, F., and K. Thermos. 2008. Effect of intravitreal administration of somatostatin and sst2 analogs on AMPA-induced neurotoxicity in rat retina. *Invest. Ophthalmol. Vis. Sci.* 49:3080–3089. https://doi.org/10.1167/iovs.07-1644

Kim, Y.H., Y.S. Kim, S.S. Kang, G.J. Cho, and W.S. Choi. 2010. Resveratrol inhibits neuronal apoptosis and elevated Ca2+/calmodulin-dependent protein kinase II activity in diabetic mouse retina. *Diabetes.* 59:1825–1835. https://doi.org/10.2337/db09-1431

Kim, Y.H., Y.S. Kim, S.Y. Park, C.H. Park, W.S. Choi, and G.J. Cho. 2011. CaMKII regulates pericyte loss in the retina of early diabetic mouse. *Mol. Cells.* 31:289–293. https://doi.org/10.1007/s10059-011-0038-2

Kopperud, R.K., C.B. Rygh, T.V. Karlsen, C. Krakstad, R. Kleppe, E.A. Hoivik, M. Bakke, O. Tenstad, F. Selheim, Å. Lidén, et al. 2017. Increased microvascular permeability in mice lacking Epac1 (Rapgef3). *Acta Physiol. (Oxf.).* 219:441–452. https://doi.org/10.1111/apha.12697

Kostic, M., M.H. Ludtmann, H. Bading, M. Hershfinkel, E. Steer, C.T. Chu, A.Y. Abramov, and I. Sekler. 2015. PKA Phosphorylation of NCLX Reverses Mitochondrial Calcium Overload and Depolarization, Promoting Survival of PINK1-Deficient Dopaminergic Neurons. *Cell Reports.* 13:376–386. https://doi.org/10.1016/j.celrep.2015.08.079

Laudette, M., A. Coluccia, Y. Sainte-Marie, A. Solari, L. Fazal, P. Sicard, R. Silvestri, J. Mialet-Perez, S. Pons, B. Ghaleb, et al. 2019. Identification of a pharmacological inhibitor of Epac1 that protects the heart against acute and chronic models of cardiac stress. *Cardiovasc. Res.* 115:1766–1777.

Li, J., P. Wang, Y. Zhu, Z. Chen, T. Shi, W. Lei, and S. Yu. 2015. Curcumin Inhibits Neuronal Loss in the Retina and Elevates Ca^{2+}/Calmodulin-Dependent Protein Kinase II Activity in Diabetic Rats. *J. Ocul. Pharmacol. Ther.* 31:555–562. https://doi.org/10.1089/jop.2015.0006

Li, L., L. Xu, W. Chen, X. Li, Q. Xia, L. Zheng, Q. Duan, H. Zhang, and Y. Zhao. 2018. Reduced Annexin A1 Secretion by ABCA1 Causes Retinal Inflammation and Ganglion Cell Apoptosis in a Murine Glaucoma Model. *Front. Cell. Neurosci.* 12:347. https://doi.org/10.3389/fncel.2018.00347

Li, M., X. Wang, M.K. Meintzer, T. Laessig, M.J. Birnbaum, and K.A. Heidenreich. 2000. Cyclic AMP promotes neuronal survival by phosphorylation of glycogen synthase kinase 3beta. *Mol. Cell. Biol.* 20:9356–9363. https://doi.org/10.1128/MCB.20.24.9356-9363.2000

Liu, L., Y. Jiang, and J.J. Steinle. 2018. Epac1 protects the retina against ischemia/reperfusion-induced neuronal and vascular damage. *PLoS One.* 13:e0204346. https://doi.org/10.1371/journal.pone.0204346

Liu, W., J. Luisi, H. Liu, M. Motamedi, and W. Zhang. 2017. OCT-Angiography for Non-Invasive Monitoring of Neuronal and Vascular Structure in Mouse Retina: Implication for Characterization of Retinal Neurovascular Coupling. *EC Ophthalmol.* 5:89–98.

Liu, W., F. Xia, Y. Ha, S. Zhu, Y. Li, O. Folorunso, A. Pashaei-Marandi, P.Y. Lin, R.G. Tilton, A.P. Pierce, et al. 2019. Neuroprotective Effects of HSF1 in Retinal Ischemia-Reperfusion Injury. *Invest. Ophthalmol. Vis. Sci.* 60:965–977. https://doi.org/10.1167/iovs.18-26216

Liu, X., P. Huang, J. Wang, Z. Yang, S. Huang, X. Luo, J. Qi, X. Shen, and Y. Zhong. 2016. The Effect of A2A Receptor Antagonist on Microglial Activation in Experimental Glaucoma. *Invest. Ophthalmol. Vis. Sci.* 57:776–786. https://doi.org/10.1167/iovs.15-18024

Liu, X., C. Ma, R. Xing, W. Zhang, B. Tian, X. Li, Q. Li, and Y. Zhang. 2013. The calmodulin-dependent protein kinase II inhibitor KN-93 protects rat cerebral cortical neurons from N-methyl-D-aspartic acid-induced injury. *Neural Regen. Res.* 8:111–120.

Liu, Y., and M.F. Schneider. 2013. Opposing HDAC4 nuclear fluxes due to phosphorylation by β-adrenergic activated protein kinase A or by activity or Epac activated CaMKII in skeletal muscle fibres. *J. Physiol.* 591:3605–3623. https://doi.org/10.1113/jphysiol.2013.256263

Lorenowicz, M.J., J. van Gils, M. de Boer, P.L. Hordijk, and M. Fernandez-Borja. 2006. Epac1-Rap1 signaling regulates monocyte adhesion and chemotaxis. *J. Leukoc. Biol.* 80:1542–1552. https://doi.org/10.1189/jlb.0506357

Madeira, M.H., R. Boia, F. Elvas, T. Martins, R.A. Cunha, A.F. Ambrósio, and A.R. Santiago. 2016. Selective A2A receptor antagonist prevents microglia-mediated neuroinflammation and protects retinal ganglion cells from high intraocular pressure-induced transient ischemic injury. *Transl. Res.* 169:112–128. https://doi.org/10.1016/j.trsl.2015.11.005

Madeira, M.H., F. Elvas, R. Boia, F.Q. Gonçalves, R.A. Cunha, A.F. Ambrósio, and A.R. Santiago. 2015. Adenosine A2AR blockade prevents neuroinflammation-induced death of retinal ganglion cells caused by elevated pressure. *J. Neuroinflammation.* 12:115. https://doi.org/10.1186/s12974-015-0333-5

Mangmool, S., A.K. Shukla, and H.A. Rockman. 2010. beta-Arrestin-dependent activation of Ca(2+)/calmodulin kinase II after beta(1)-adrenergic receptor stimulation. *J. Cell Biol.* 189:573–587. https://doi.org/10.1083/jcb.200911047

Métrich, M., A. Lucas, M. Gastineau, J.L. Samuel, C. Heymes, E. Morel, and F. Lezoualc'h. 2008. Epac mediates beta-adrenergic receptor-induced cardiomyocyte hypertrophy. *Circ. Res.* 102:959–965. https://doi.org/10.1161/CIRCRESAHA.107.164947

Moore, T.C., J.E. Moore, Y. Kaji, N. Frizzell, T. Usui, V. Poulaki, I.L. Campbell, A.W. Stitt, T.A. Gardiner, D.B. Archer, and A.P. Adamis. 2003. The role of advanced glycation end products in retinal microvascular leukostasis. *Invest. Ophthalmol. Vis. Sci.* 44:4457–4464. https://doi.org/10.1167/iovs.02-1063

Nishijima, K., Y.S. Ng, L. Zhong, J. Bradley, W. Schubert, N. Jo, J. Akita, S.J. Samuelsson, G.S. Robinson, A.P. Adamis, and D.T. Shima. 2007. Vascular endothelial growth factor-A is a survival factor for retinal neurons and a critical neuroprotectant during the adaptive response to ischemic injury. *Am. J. Pathol.* 171:53–67. https://doi.org/10.2353/ajpath.2007.061237

Oestreich, E.A., S. Malik, S.A. Goonasekera, B.C. Blaxall, G.G. Kelley, R.T. Dirksen, and A.V. Smrcka. 2009. Epac and phospholipase Cepsilon regulate Ca2+ release in the heart by activation of protein kinase Cepsilon and calcium-calmodulin kinase II. *J. Biol. Chem.* 284:1514–1522. https://doi.org/10.1074/jbc.M806994200

Ohnuki, Y., D. Umeki, Y. Mototani, H. Jin, W. Cai, K. Shiozawa, K. Suita, Y. Saeki, T. Fujita, Y. Ishikawa, and S. Okumura. 2014. Role of cyclic AMP sensor Epac1 in masseter muscle hypertrophy and myosin heavy chain transition induced by β2-adrenoceptor stimulation. *J. Physiol.* 592:5461–5475. https://doi.org/10.1113/jphysiol.2014.282996

Okumura, S., T. Fujita, W. Cai, M. Jin, I. Namekata, Y. Mototani, H. Jin, Y. Ohnuki, Y. Tsuneoka, R. Kurotani, et al. 2014. Epac1-dependent phospholamban phosphorylation mediates the cardiac response to stresses. *J. Clin. Invest.* 124:2785–2801. https://doi.org/10.1172/JCI64784

Pereira, L., M. Métrich, M. Fernández-Velasco, A. Lucas, J. Leroy, R. Perrier, E. Morel, R. Fischmeister, S. Richard, J.P. Bénitah, et al. 2007. The cAMP binding protein Epac modulates Ca2+ sparks by a Ca2+/calmodulin kinase signalling pathway in rat cardiac myocytes. *J. Physiol.* 583:685–694. https://doi.org/10.1113/jphysiol.2007.133066

Pereira, L., H. Rehmann, D.H. Lao, J.R. Erickson, J. Bossuyt, J. Chen, and D.M. Bers. 2015. Novel Epac fluorescent ligand reveals distinct Epac1 vs. Epac2 distribution and function in cardiomyocytes. *Proc. Natl. Acad. Sci. USA.* 112:3991–3996. https://doi.org/10.1073/pnas.1416163112

Robichaux, W.G. III, and X. Cheng. 2018. Intracellular cAMP Sensor EPAC: Physiology, Pathophysiology, and Therapeutics Development. *Physiol. Rev.* 98:919–1053. https://doi.org/10.1152/physrev.00025.2017

Rojas, M., W. Zhang, D.L. Lee, M.J. Romero, D.T. Nguyen, M. Al-Shabrawey, N.T. Tsai, G.I. Liou, M.W. Brands, R.W. Caldwell, and R.B. Caldwell. 2010. Role of IL-6 in angiotensin II-induced retinal vascular inflammation. *Invest. Ophthalmol. Vis. Sci.* 51:1709–1718. https://doi.org/10.1167/iovs.09-3375

Sappington, R.M., B.J. Carlson, S.D. Crish, and D.J. Calkins. 2010. The microbead occlusion model: a paradigm for induced ocular hypertension in rats and mice. *Invest. Ophthalmol. Vis. Sci.* 51:207–216. https://doi.org/10.1167/iovs.09-3947

Saszik, S.M., J.G. Robson, and L.J. Frishman. 2002. The scotopic threshold response of the dark-adapted electroretinogram of the mouse. *J. Physiol.* 543:899–916. https://doi.org/10.1113/jphysiol.2002.019703

Schmidt, M., F.J. Dekker, and H. Maarsingh. 2013. Exchange protein directly activated by cAMP (epac): a multidomain cAMP mediator in the regulation of diverse biological functions. *Pharmacol. Rev.* 65:670–709. https://doi.org/10.1124/pr.110.003707

Scott, J., G.J. Harris, E.M. Pinder, J.G. Macfarlane, T.P. Hellyer, A.J. Rostron, A. Conway Morris, D.R. Thickett, G.D. Perkins, D.F. McAuley, et al. 2016. Exchange protein directly activated by cyclic AMP (EPAC) activation reverses neutrophil dysfunction induced by β2-agonists, corticosteroids, and critical illness. *J. Allergy Clin. Immunol.* 137:535–544.

Shosha, E., Z. Xu, H. Yokota, A. Saul, M. Rojas, R.W. Caldwell, R.B. Caldwell, and S.P. Narayanan. 2016. Arginase 2 promotes neurovascular

degeneration during ischemia/reperfusion injury. *Cell Death Dis.* 7: e2483. https://doi.org/10.1038/cddis.2016.295

Singhmar, P., X. Huo, N. Eijkelkamp, S.R. Berciano, F. Baameur, F.C. Mei, Y. Zhu, X. Cheng, D. Hawke, F. Mayor Jr., et al. 2016. Critical role for Epac1 in inflammatory pain controlled by GRK2-mediated phosphorylation of Epac1. *Proc. Natl. Acad. Sci. USA.* 113:3036–3041.

Singhmar, P., X. Huo, Y. Li, P.M. Dougherty, F. Mei, X. Cheng, C.J. Heijnen, and A. Kavelaars. 2018. Orally active Epac inhibitor reverses mechanical allodynia and loss of intraepidermal nerve fibers in a mouse model of chemotherapy-induced peripheral neuropathy. *Pain.* 159:884–893. https://doi.org/10.1097/j.pain.0000000000001160

Skowronska-Krawczyk, D., L. Zhao, J. Zhu, R.N. Weinreb, G. Cao, J. Luo, K. Flagg, S. Patel, C. Wen, M. Krupa, et al. 2015. P16INK4a Upregulation Mediated by SIX6 Defines Retinal Ganglion Cell Pathogenesis in Glaucoma. *Mol. Cell.* 59:931–940. https://doi.org/10.1016/j.molcel.2015.07.027

Srinivas, S., T. Watanabe, C.S. Lin, C.M. William, Y. Tanabe, T.M. Jessell, and F. Costantini. 2001. Cre reporter strains produced by targeted insertion of EYFP and ECFP into the ROSA26 locus. *BMC Dev. Biol.* 1:4. https://doi.org/10.1186/1471-213X-1-4

Srivastava, D.P., K.A. Jones, K.M. Woolfrey, J. Burgdorf, T.A. Russell, A. Kalmbach, H. Lee, C. Yang, M.M. Bradberry, D. Wokosin, et al. 2012. Social, communication, and cortical structural impairments in Epac2-deficient mice. *J. Neurosci.* 32:11864–11878. https://doi.org/10.1523/JNEUROSCI.1349-12.2012

Sun, M.H., J.H. Pang, S.L. Chen, W.H. Han, T.C. Ho, K.J. Chen, L.Y. Kao, K.K. Lin, and Y.P. Tsao. 2010. Retinal protection from acute glaucoma-induced ischemia-reperfusion injury through pharmacologic induction of heme oxygenase-1. *Invest. Ophthalmol. Vis. Sci.* 51:4798–4808. https://doi.org/10.1167/iovs.09-4086

Suzuki, S., U. Yokoyama, T. Abe, H. Kiyonari, N. Yamashita, Y. Kato, R. Kurotani, M. Sato, S. Okumura, and Y. Ishikawa. 2010. Differential roles of Epac in regulating cell death in neuronal and myocardial cells. *J. Biol. Chem.* 285:24248–24259. https://doi.org/10.1074/jbc.M109.094581

Taylor, S.S., P. Zhang, J.M. Steichen, M.M. Keshwani, and A.P. Kornev. 2013. PKA: lessons learned after twenty years. *Biochim. Biophys. Acta.* 1834: 1271–1278. https://doi.org/10.1016/j.bbapap.2013.03.007

Timmins, J.M., L. Ozcan, T.A. Seimon, G. Li, C. Malagelada, J. Backs, T. Backs, R. Bassel-Duby, E.N. Olson, M.E. Anderson, and I. Tabas. 2009. Calcium/calmodulin-dependent protein kinase II links ER stress with Fas and mitochondrial apoptosis pathways. *J. Clin. Invest.* 119:2925–2941. https://doi.org/10.1172/JCI38857

Toledo, F.D., L.M. Pérez, C.L. Basiglio, J.E. Ochoa, E.J. Sanchez Pozzi, and M.G. Roma. 2014. The Ca^{2+}-calmodulin-Ca^{2+}/calmodulin-dependent protein kinase II signaling pathway is involved in oxidative stress-induced mitochondrial permeability transition and apoptosis in isolated rat hepatocytes. *Arch. Toxicol.* 88:1695–1709. https://doi.org/10.1007/s00204-014-1219-5

Unal Cevik, I., and T. Dalkara. 2003. Intravenously administered propidium iodide labels necrotic cells in the intact mouse brain after injury. *Cell Death Differ.* 10:928–929. https://doi.org/10.1038/sj.cdd.4401250

Varma, R., P. Peeples, J.G. Walt, and T.J. Bramley. 2008. Disease progression and the need for neuroprotection in glaucoma management. *Am. J. Manag. Care.* 14(1, Suppl):S15–S19.

Vliem, M.J., B. Ponsioen, F. Schwede, W.J. Pannekoek, J. Riedl, M.R. Kooistra, K. Jalink, H.G. Genieser, J.L. Bos, and H. Rehmann. 2008. 8-pCPT-2′-O-Me-cAMP-AM: an improved Epac-selective cAMP analogue. *ChemBioChem.* 9:2052–2054. https://doi.org/10.1002/cbic.200800216

Wan, P., W. Su, Y. Zhang, Z. Li, C. Deng, and Y. Zhuo. 2017. Trimetazidine protects retinal ganglion cells from acute glaucoma via the Nrf2/Ho-1 pathway. *Clin. Sci. (Lond.).* 131:2363–2375. https://doi.org/10.1042/CS20171182

Wang, H., C.J. Heijnen, C.T. van Velthoven, H.L. Willemen, Y. Ishikawa, X. Zhang, A.K. Sood, A. Vroon, N. Eijkelkamp, and A. Kavelaars. 2013. Balancing GRK2 and EPAC1 levels prevents and relieves chronic pain. *J. Clin. Invest.* 123:5023–5034. https://doi.org/10.1172/JCI66241

Weinreb, R.N., T. Aung, and F.A. Medeiros. 2014. The pathophysiology and treatment of glaucoma: a review. *JAMA.* 311:1901–1911. https://doi.org/10.1001/jama.2014.3192

Whitaker, C.M., and N.G. Cooper. 2010. Differential distribution of exchange proteins directly activated by cyclic AMP within the adult rat retina. *Neuroscience.* 165:955–967. https://doi.org/10.1016/j.neuroscience.2009.10.054

Yan, J., F.C. Mei, H. Cheng, D.H. Lao, Y. Hu, J. Wei, I. Patrikeev, D. Hao, S.J. Stutz, K.T. Dineley, et al. 2013. Enhanced leptin sensitivity, reduced adiposity, and improved glucose homeostasis in mice lacking exchange protein directly activated by cyclic AMP isoform 1. *Mol. Cell. Biol.* 33: 918–926. https://doi.org/10.1128/MCB.01227-12

Yang, Q., K.S. Cho, H. Chen, D. Yu, W.H. Wang, G. Luo, I.H. Pang, W. Guo, and D.F. Chen. 2012a. Microbead-induced ocular hypertensive mouse model for screening and testing of aqueous production suppressants for glaucoma. *Invest. Ophthalmol. Vis. Sci.* 53:3733–3741. https://doi.org/10.1167/iovs.12-9814

Yang, Y., X. Shu, D. Liu, Y. Shang, Y. Wu, L. Pei, X. Xu, Q. Tian, J. Zhang, K. Qian, et al. 2012b. EPAC null mutation impairs learning and social interactions via aberrant regulation of miR-124 and Zif268 translation. *Neuron.* 73:774–788. https://doi.org/10.1016/j.neuron.2012.02.003

Ye, N., Y. Zhu, H. Chen, Z. Liu, F.C. Mei, C. Wild, H. Chen, X. Cheng, and J. Zhou. 2015. Structure-Activity Relationship Studies of Substituted 2-(Isoxazol-3-yl)-2-oxo-N′-phenyl-acetohydrazonoyl Cyanide Analogues: Identification of Potent Exchange Proteins Directly Activated by cAMP (EPAC) Antagonists. *J. Med. Chem.* 58:6033–6047. https://doi.org/10.1021/acs.jmedchem.5b00635

Zhang, C.L., M. Katoh, T. Shibasaki, K. Minami, Y. Sunaga, H. Takahashi, N. Yokoi, M. Iwasaki, T. Miki, and S. Seino. 2009. The cAMP sensor Epac2 is a direct target of antidiabetic sulfonylurea drugs. *Science.* 325: 607–610. https://doi.org/10.1126/science.1172256

Zhang, H., J.H. Park, S. Maharjan, J.A. Park, K.S. Choi, H. Park, Y. Jeong, J.H. Ahn, I.H. Kim, J.C. Lee, et al. 2017. Sac-1004, a vascular leakage blocker, reduces cerebral ischemia-reperfusion injury by suppressing blood-brain barrier disruption and inflammation. *J. Neuroinflammation.* 14:122. https://doi.org/10.1186/s12974-017-0897-3

Zhang, T., Y. Zhang, M. Cui, L. Jin, Y. Wang, F. Lv, Y. Liu, W. Zheng, H. Shang, J. Zhang, et al. 2016. CaMKII is a RIP3 substrate mediating ischemia- and oxidative stress-induced myocardial necroptosis. *Nat. Med.* 22:175–182. https://doi.org/10.1038/nm.4017

Zhu, Y., H. Chen, S. Boulton, F. Mei, N. Ye, G. Melacini, J. Zhou, and X. Cheng. 2015. Biochemical and pharmacological characterizations of ESI-09 based EPAC inhibitors: defining the ESI-09 “therapeutic window”. *Sci. Rep.* 5:9344. https://doi.org/10.1038/srep09344

Supplemental material

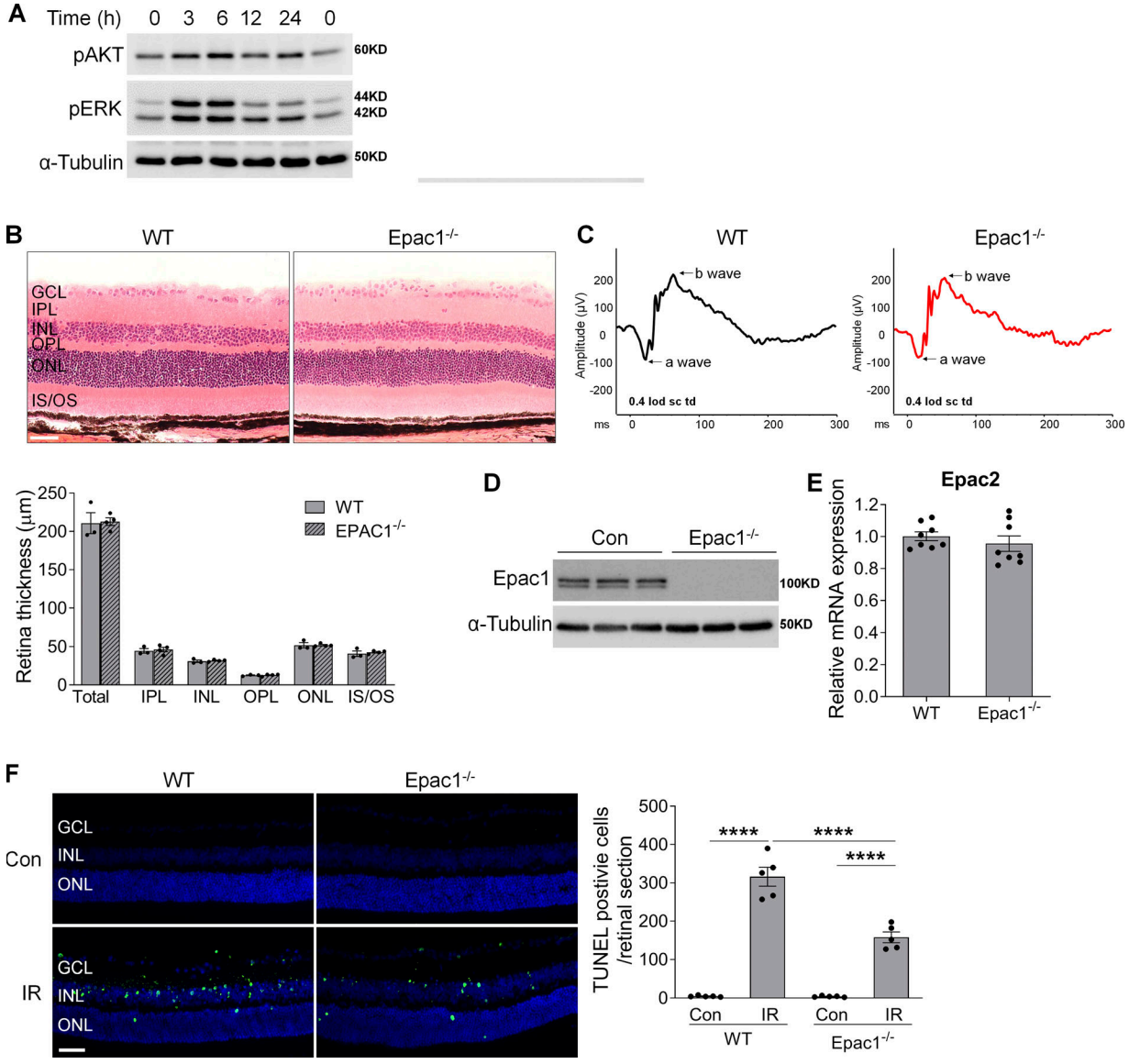

Figure S1. **Examination of downstream targets of Epac1 signaling after ischemic injury and characterization of the retina of *Epac1*$^{-/-}$ mice.** **(A)** Phosphorylation of AKT and ERK in WT retinas at various time points after ischemia injury. **(B)** Eyeballs were collected from WT and *Epac1*$^{-/-}$ mice for retinal structure in H&E-stained retinal sections. Bar graph represents quantification of the thickness of total retina and individual retinal layers. *n* = 3–4 mice. Scale bar: 50 μm. **(C)** Representative graphs of the a-wave and b-wave amplitude from ERG recordings of WT and *Epac1*$^{-/-}$ mice. **(D)** Epac1 protein expression by Western blot analysis. *n* = 3 mice. **(E)** Epac2 mRNA expression by quantitative PCR. *n* = 8 mice. **(F)** *Epac1* deletion reduces apoptotic cell death after IR. TUNEL assay was conducted on retinal frozen sections 24 h after IR in WT and *Epac1*$^{-/-}$ mice. Green, TUNEL-positive cells; blue, DAPI staining of nuclei. Bar graph represents the number of apoptotic cells per retinal section. *n* = 5 mice; TUNEL-positive cells in three retinal sections for each sample were counted under microscope and calculated as average value. ****, P < 0.0001; one-way ANOVA. Scale bar: 50 μm. IPL, inner plexiform layer; IS/OS: inner segment/outer segment; ONL, outer nuclear layer; OPL, outer plexiform layer. Error bars represent SEM.

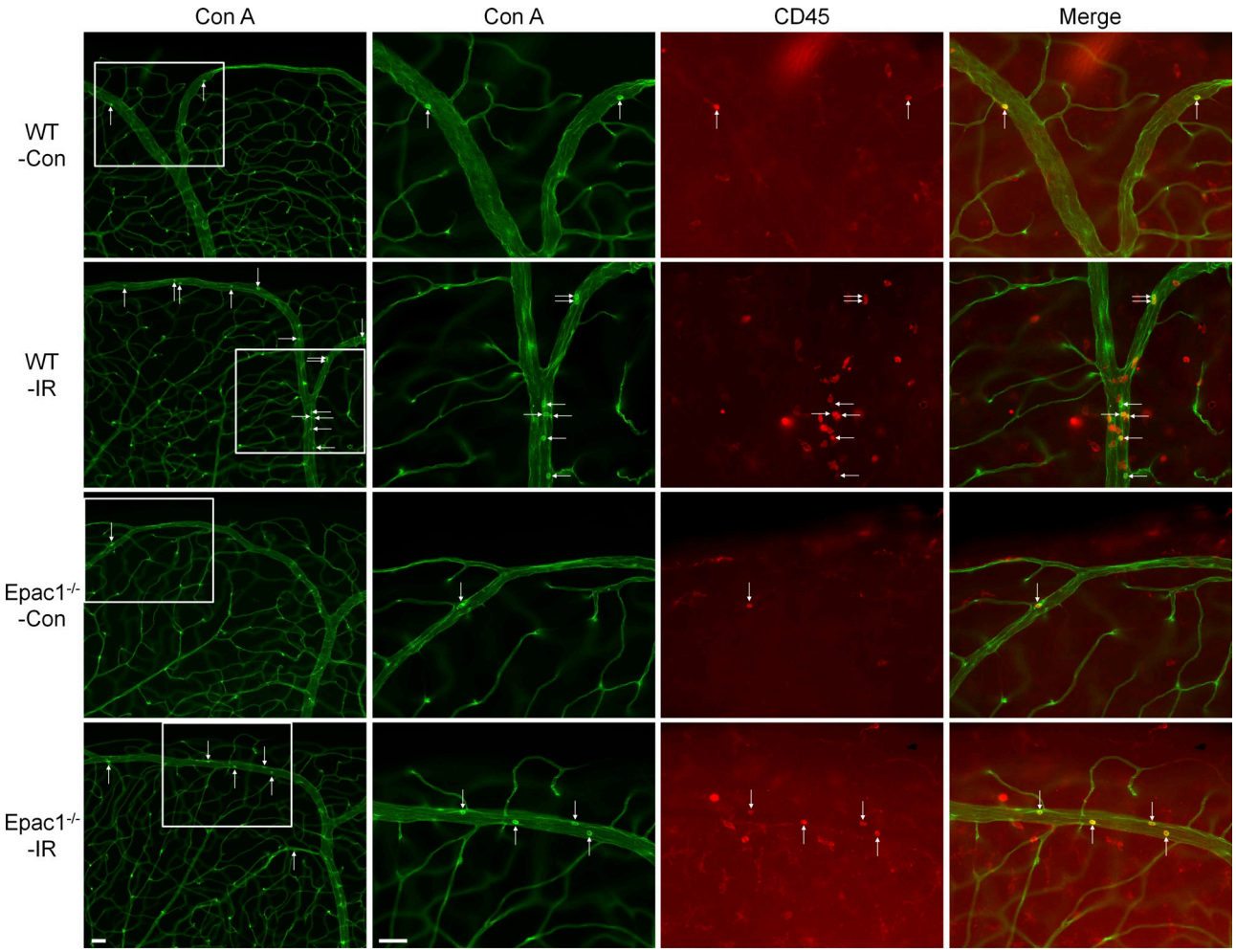

Figure S2. ***Epac1* deletion decreases leukostasis in the retina after IR injury.** Representative images of leukostasis in the peripheral retinas. WT and *Epac1*$^{-/-}$ mice were subjected to IR, and leukostasis assay was performed 24 h after IR. Green, Con A–labeled retinal vasculature and adherent leukocytes. Red, CD45 immunostaining for leukocytes. Rectangles in the left rows of images are zoomed in, and arrows indicate stationary leukocytes adherent to the vascular endothelium. Scale bar: 50 µm. *n* = 5–6 mice. Error bars represent SEM.

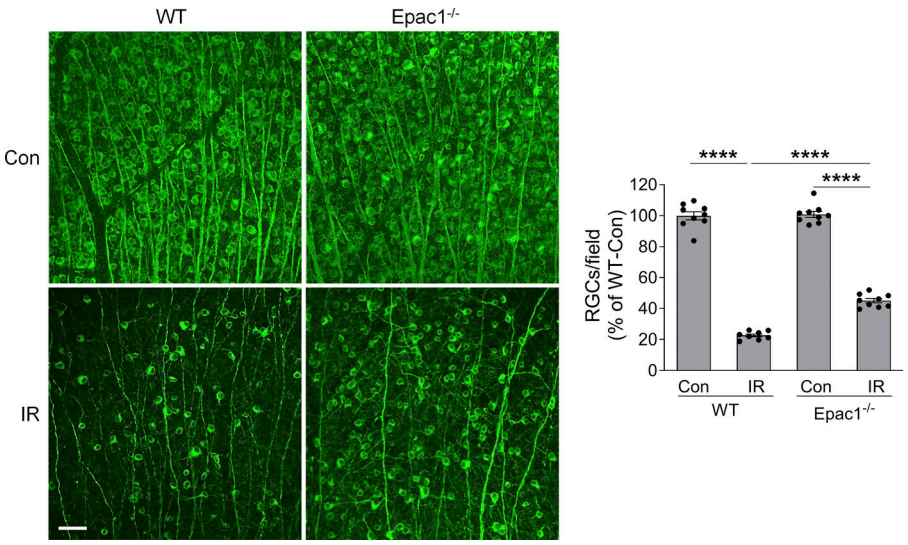

Figure S3. ***Epac1* deletion prevents RGC loss 14 d after IR.** Representative images of retinal flatmounts labeled with Tuj1 antibody (green) 14 d after IR in WT and *Epac1*$^{-/-}$ mice. Bar graph represents the number of Tuj1-positive cells per field. Scale bar: 50 µm. *n* = 8–9 mice; eight images were taken at the peripheral retina for each sample and calculated as average value. ****, P < 0.0001; one-way ANOVA. Error bars represent SEM.

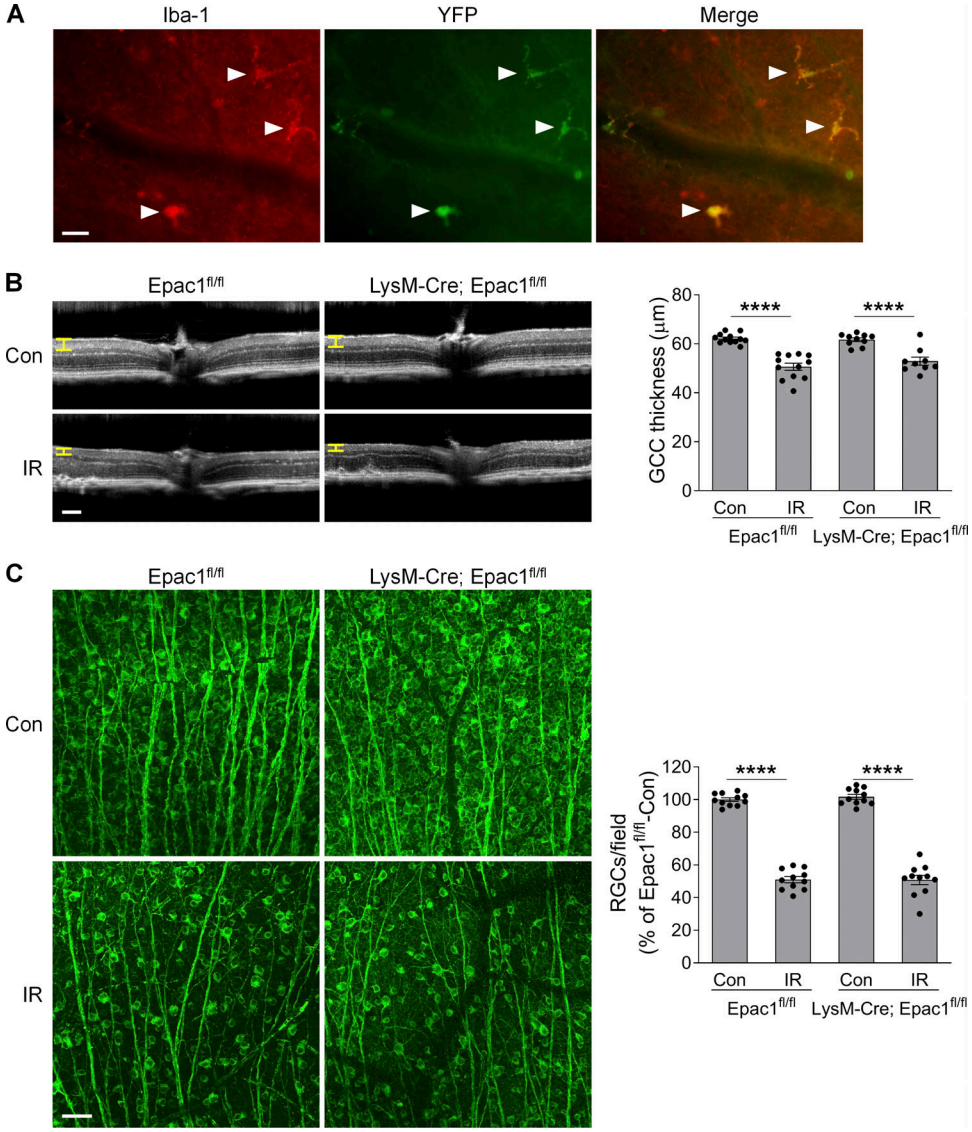

Figure S4. ***Epac1* deletion in myeloid cells does not affect RGC death after IR. (A)** LysM-Cre mice were crossed with Rosa26YFP reporter mice to generate LysM-Cre; Rosa26YFP mice. Retinal flatmounts were stained with antibodies against YFP (green) and microglial marker Iba1 (red). Arrows indicate microglia. Scale bar: 25 μm. **(B)** OCT analysis in live *Epac1*$^{fl/fl}$ and LysM-Cre; *Epac1*$^{fl/fl}$ mice for retinal thickness 7 d after IR. Yellow H lines indicate the thickness of GCC. Bar graph represents the thickness of GCC. *n* = 10–12 mice. Scale bar: 100 μm. **(C)** Representative images of retinal flatmounts labeled with Tuj1 antibody (green) in *Epac1*$^{fl/fl}$ and LysM-Cre; *Epac1*$^{fl/fl}$ mice 7 d after IR. Scale bar: 50 μm. Bar graph represents the number of Tuj1-positive cells per field. *n* = 11 mice; eight images were taken at the peripheral retina for each sample and calculated as average value. ****, P < 0.0001; one-way ANOVA. Error bars represent SEM.

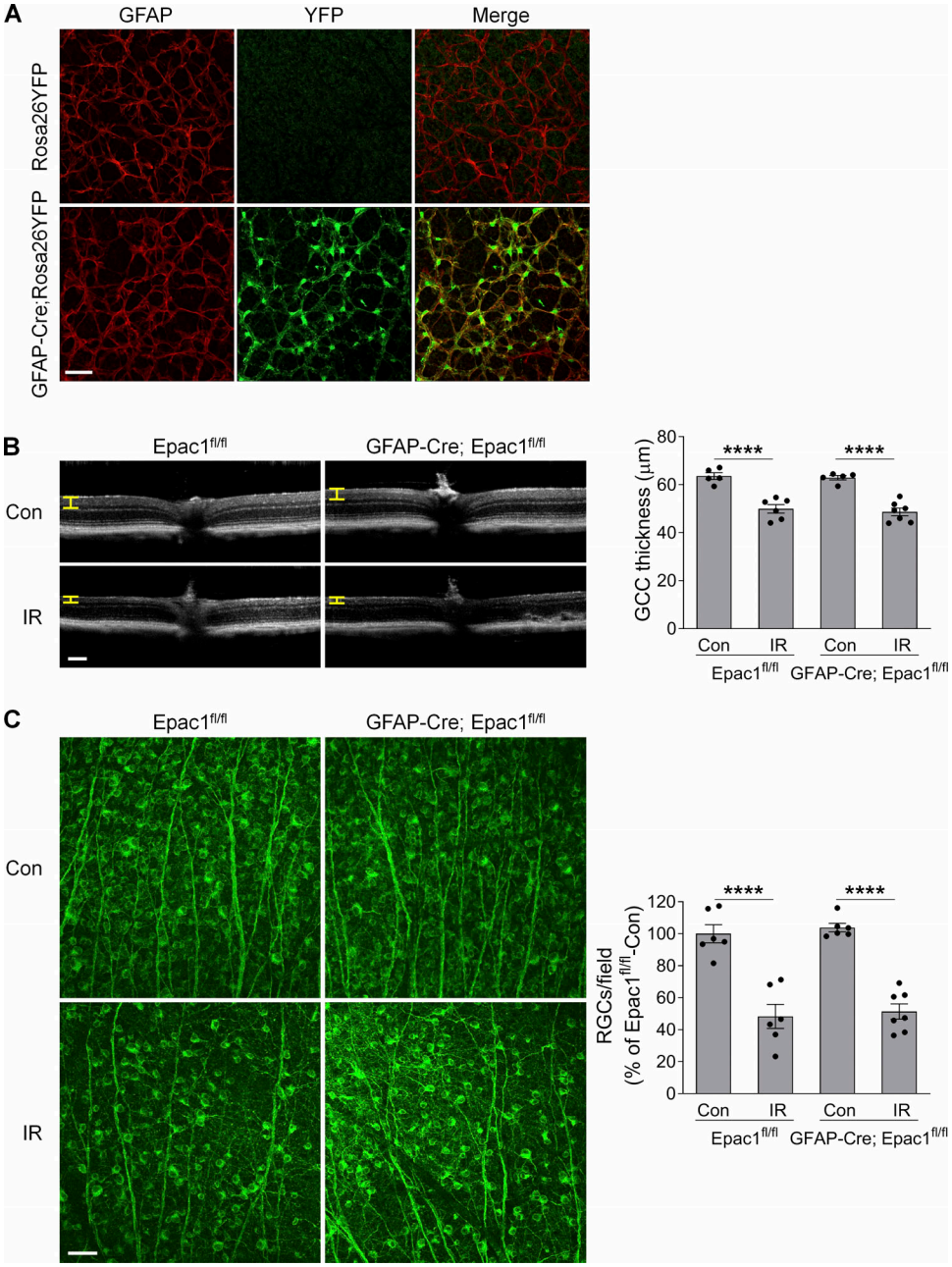

Figure S5. ***Epac1* deletion in astrocytes does not affect RGC death after IR. (A)** GFAP-Cre mice were crossed with Rosa26YFP reporter mice to generate GFAP-Cre; Rosa26YFP mice. Retinal flatmounts were stained with antibodies against YFP (green) and astrocyte marker GFAP (red). **(B)** OCT analysis in live *Epac1*$^{fl/fl}$ and GFAP-Cre; *Epac1*$^{fl/fl}$ mice for retinal thickness 7 d after IR. Yellow H lines indicate the thickness of GCC. Bar graph represents the thickness of GCC. n = 5–7 mice. Scale bar: 100 µm. **(C)** Representative images of retinal flatmounts labeled with Tuj1 antibody (green) in *Epac1*$^{fl/fl}$ and GFAP-Cre; *Epac1*$^{fl/fl}$ mice 7 d after IR. Scale bar: 50 µm. Bar graph represents the number of Tuj1-positive cells per field. n = 6–7 mice; eight images were taken at the peripheral retina for each sample and calculated as average value. ****, P < 0.0001; one-way ANOVA. Error bars represent SEM.